Journal of Medicinal Chemistry

pubs.acs.org/jmc

Article

Expedited Approach toward the Rational Design of Noncovalent SARS-CoV-2 Main Protease Inhibitors

Naoya Kitamura, Michael Dominic Sacco, Chunlong Ma, Yanmei Hu, Julia Alma Townsend, Xiangzhi Meng, Fushun Zhang, Xiujun Zhang, Mandy Ba, Tommy Szeto, Adis Kukuljac, Michael Thomas Marty, David Schultz, Sara Cherry, Yan Xiang, Yu Chen,* and Jun Wang*

Cite This: J. Med. Chem. 2022, 65, 2848−2865

Read Online

ACCESS | Metrics & More | Article Recommendations | Supporting Information

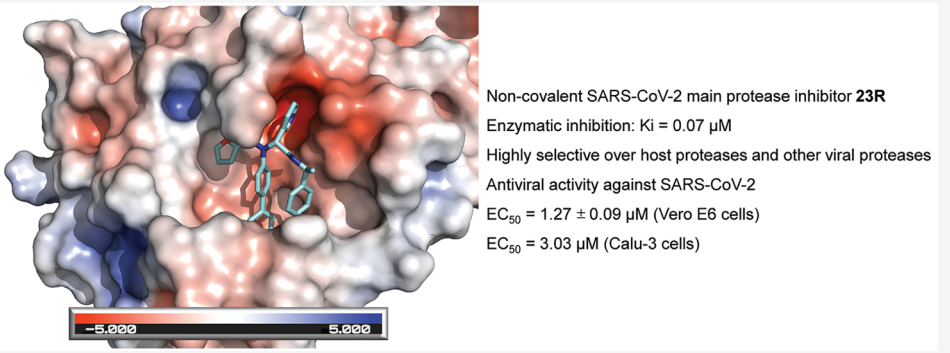

ABSTRACT: The main protease (M^{pro}) of SARS-CoV-2 is a validated antiviral drug target. Several M^{pro} inhibitors have been reported with potent enzymatic inhibition and cellular antiviral activity, including **GC376**, **boceprevir**, **calpain inhibitors II**, and **XII**, with each containing a reactive warhead that covalently modifies the catalytic Cys145. Coupling structure-based drug design with the one-pot Ugi four-component reaction, we discovered one of the most potent noncovalent inhibitors, **23R** (**Jun8-76-3A**) that is structurally distinct from the canonical M^{pro} inhibitor **GC376**. Significantly, **23R** is highly selective compared with covalent inhibitors such as **GC376**, especially toward host proteases. The cocrystal structure of SARS-CoV-2 M^{pro} with **23R** revealed a previously unexplored binding site located in between the S2 and S4 pockets. Overall, this study discovered **23R**, one of the most potent and selective noncovalent SARS-CoV-2 M^{pro} inhibitors reported to date, and a novel binding pocket in M^{pro} that can be explored for inhibitor design.

INTRODUCTION

The COVID-19 pandemic had a significant impact on the global economy and public health, and there is an urgent need for therapeutic interventions. The viral polymerase inhibitor remdesivir gained FDA approval on October 22nd, 2020. The combination therapy of remdesivir with the Janus kinase (JAK) inhibitor baricitinib also received FDA emergency use authorization.[1] Among the other drug targets being pursued at preclinical and clinical stages,[2] the viral main protease (M^{pro}), also called 3-chymotrypsin-like protease ($3CL^{pro}$), is one of the most extensively explored high profile antiviral drug targets.[3] M^{pro} is a cysteine protease encoded in the viral polyprotein as nonstructural protein 5 (Nsp5) that cleaves the viral polyproteins pp1a and pp1ab at more than 11 sites. Despite its multiple proteolytic sites, M^{pro} was shown to have a high substrate specificity of glutamine at the P1 position.[4] As such, the majority of the reported M^{pro} inhibitors were designed to contain a 2-pyrrolidone at the P1 substitution as a mimetic of the glutamine in the substrate.[5] Most advanced M^{pro} inhibitors including **PF-07304814**,[6] **GC376**,[7,8] **6j**,[9] **MI-09**, and **MI-30**[10] all belong to this category (Figure 1). **PF-07304814**, an α-hydroxyl ketone prodrug, is being developed by Pfizer and has optimal pharmacokinetic properties and recently entered human clinical trials.[6] **GC376** has *in vivo* antiviral efficacy in treating cats infected with lethal feline infectious peritonitis virus.[11,12] Recently, the **GC376** analog **6j** was shown to protect mice from MERS-CoV infection.[9] **MI-09** and **MI-30** were shown to protect mice from lethal SARS-CoV-2 infection.[10] These promising results highlight the translational potential of M^{pro} inhibitors as potent SARS-CoV-2 antivirals and validate M^{pro} as an antiviral drug target for coronaviruses.

Special Issue: COVID-19

Received: March 19, 2021
Published: April 23, 2021

https://doi.org/10.1021/acs.jmedchem.1c00509
J. Med. Chem. 2022, 65, 2848−2865

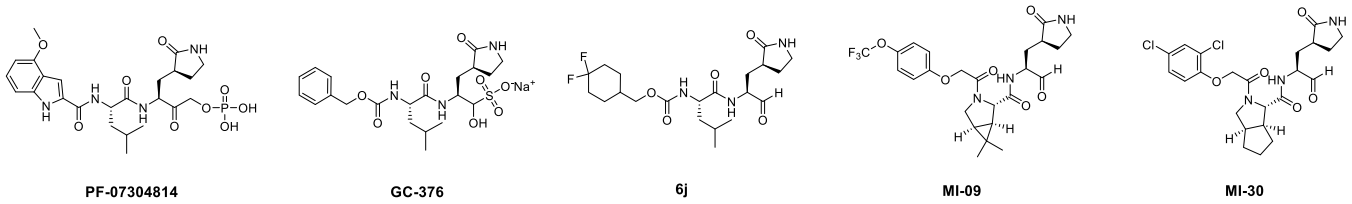

Figure 1. Promising SARS-CoV-2 M^{pro} inhibitors reported in the literature with translational potential.

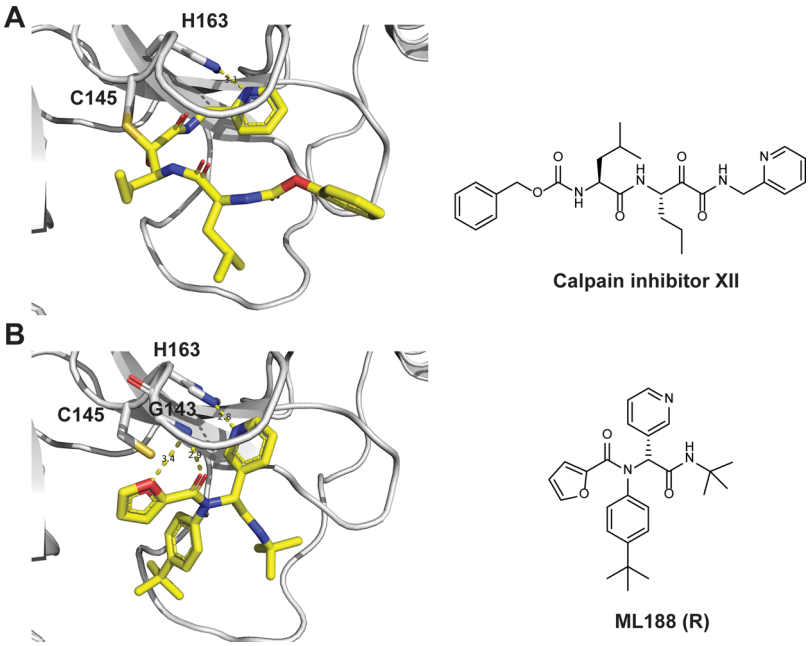

Figure 2. Structure of M^{pro} with inhibitors. (A) X-ray crystal structure of SARS-CoV-2 M^{pro} in complex with **calpain inhibitor XII** (PDB: 6XFN). (B) X-ray crystal structure of SARS-Co-V M^{pro} in complex with **ML188 (R)** (PDB: 3V3M). Hydrogen bonds are shown in dashed lines.

Drug discovery is a lengthy process involving iterative cycles of design, synthesis, and pharmacological characterization. In the event of the COVID-19 pandemic, an expedited approach with a fast turnover of this development cycle is highly desired. Using SARS-CoV-2 M^{pro} as a drug target, we report herein a fast-track drug discovery approach by coupling structure-based drug design and the Ugi four-component reaction (Ugi-4CR) methodology. The design was based on the superimposed structures of SARS-CoV or SARS-CoV-2 M^{pro} in complex with inhibitors including **GC376**, **calpain inhibitor XII**, and **ML188 (R)**.[7,8,13] The lead compound **23R** from this study is the most potent noncovalent SARS-CoV-2 M^{pro} inhibitor reported to date in terms of enzymatic inhibition and cellular antiviral activity. The target selectivity of the designed inhibitors was profiled against a panel of viral proteases and host proteases, and the noncovalent inhibitor **23R** was found to be highly selective compared to the covalent inhibitor **GC376**. An X-ray crystal structure of SARS-CoV-2 M^{pro} in complex with **23R** was solved, revealing a drug-induced conformational change and a previously unexplored binding site in between the S2 and S4 pockets. Overall, this study led to the discovery of the noncovalent M^{pro} inhibitor **23R** with potent enzymatic inhibition and *in vitro* cellular antiviral activity with a novel mechanism of action.

RESULTS AND DISCUSSION

Rational Design of Noncovalent SARS-CoV-2 M^{pro} Inhibitors. Among the noncanonical SARS-CoV-2 M^{pro} inhibitors we recently discovered, **calpain inhibitor XII** has an unexpected binding mode showing an inverted conformation in the active site (Figure 2A).[8] Instead of projecting the norvaline and leucine side chains into the S1 and S2 pockets as one would expect from its chemical structure, the pyridinyl substitution snuggly fits in the S1 pocket and forms a hydrogen bond with the H163 imidazole (Figure 2A). This hydrogen bond is essential, as replacing the pyridine with benzene led to an analog **UAWJ257** with a significant loss of enzymatic inhibition.[8] Examining the X-ray crystal structures of SARS-CoV and SARS-CoV-2 M^{pro} in the PDB database revealed another compound **ML188 (R)**,[13] which shares a similar binding mode with **calpain inhibitor XII**. **ML188 (R)** is a noncovalent SARS-CoV M^{pro} inhibitor derived from a high-throughput screening hit.[13] The pyridinyl from **ML188 (R)** similarly fits in the S1 pocket and forms a hydrogen bond with the H163 side chain imidazole (Figure 2B). In addition, the furyl oxygen and its amide oxygen both form a hydrogen bond with the G143 main chain amide amine. **ML188 (R)** was reported to inhibit the SARS-CoV M^{pro} with an IC_{50} value of 1.5 ± 0.3 μM and the SARS-CoV viral replication in Vero E6 cells with an EC_{50} value of 12.9 μM.[13] Several follow up studies have been conducted to optimize the enzymatic inhibition and cellular antiviral activity of this series of compounds; however, no significant improvement has been made.[14,15]

The similar binding mode of **ML188 (R)** with **calpain inhibitor XII**, coupled with the convenient synthesis through the one pot Ugi-4CR, inspired us to design noncovalent SARS-

https://doi.org/10.1021/acs.jmedchem.1c00509
J. Med. Chem. 2022, 65, 2848−2865

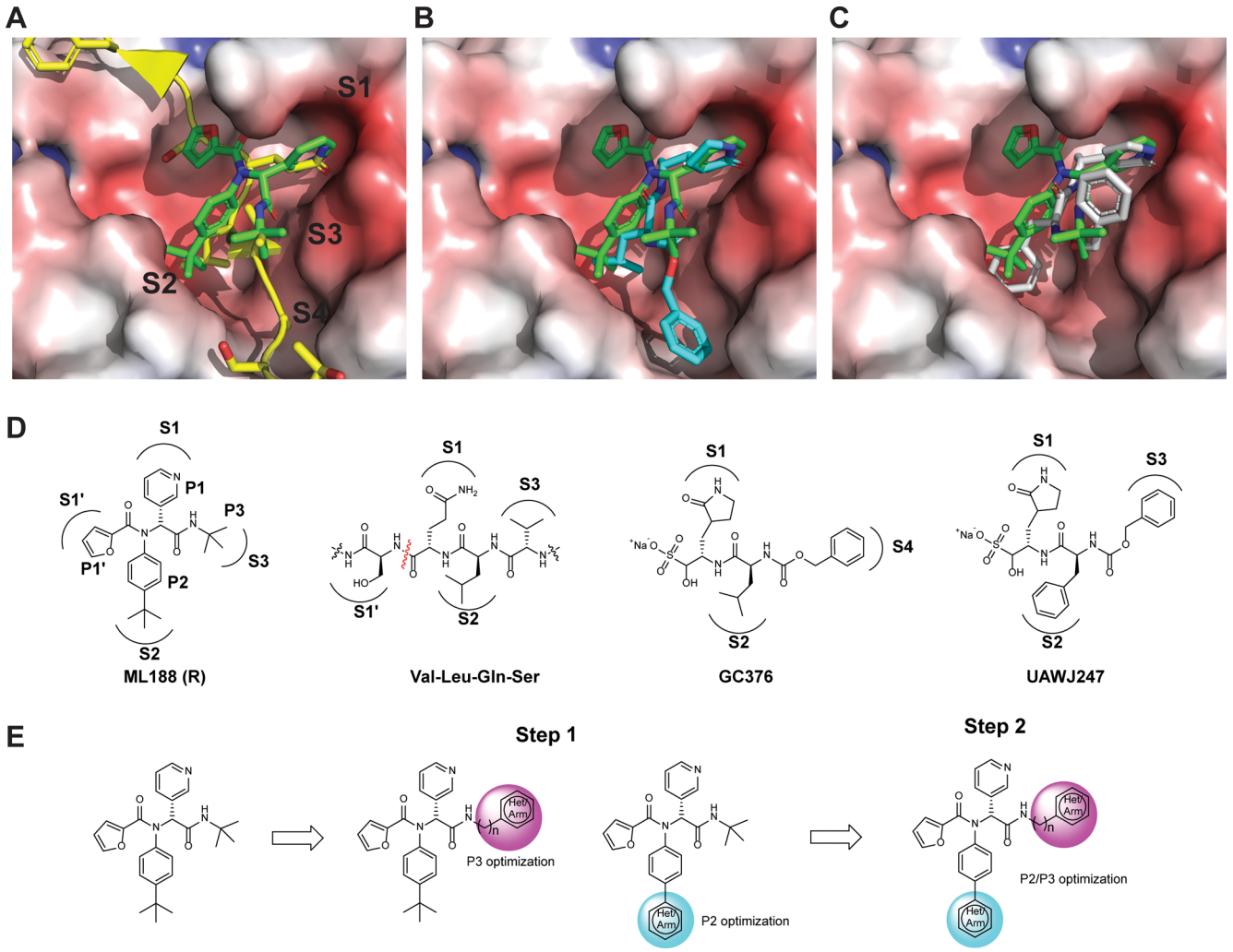

Figure 3. Design rationale for the noncovalent SARS-CoV-2 M^{pro} inhibitors. (A) Superimposed X-ray crystal structures of SARS-CoV M^{pro} + ML188 (R) (PDB: 3V3M, green) and SARS-CoV M^{pro} H41A mutant + peptide substrate (PDB: 2Q6G, yellow with backbone shown as ribbon representation). (B) Superimposed X-ray crystal structures of SARS-CoV M^{pro} + **ML188 (R)** (PDB: 3V3M) and SARS-CoV-2 M^{pro} + **GC376** (PDB: 6WTT). (C) Superimposed X-ray crystal structures of SARS-CoV M^{pro} + **ML188 (R)** (PDB: 3V3M) and SARS-CoV-2 M^{pro} + **UAWJ247** (PDB: 6XBH). (D) Chemical structures of **ML188 (R)**, peptide substrate VLQS, **GC376**, and **UAWJ247**. (E) Stepwise optimization of **ML188 (R)** toward potent noncovalent SARS-CoV-2 M^{pro} inhibitor.

CoV-2 M^{pro} inhibitors based on the **ML188 (R)** scaffold. Specifically, we leverage our understanding of the M^{pro} inhibition mechanism based on the X-ray crystal structures of SARS-CoV-2 M^{pro} with multiple inhibitors to guide the lead optimization (Figure 3A–D).[7,8] Overlaying the X-ray crystal structures of SARS-CoV M^{pro} + **ML188 (R)** (PDB: 3V3M) and the SARS-CoV M^{pro} H41A mutant + the peptide substrate (PDB: 2Q6G) revealed that the furyl, 4-*tert*-butylphenyl, pyridinyl, and *tert*-butyl of **ML188 (R)** fit in the S1′, S2, S1, and S3 pockets, respectively (Figure 3A, D). Therefore, the furyl, 4-*tert*-butylphenyl, pyridinyl, and *tert*-butyl substitutions in **ML188 (R)** were defined as P1′, P2, P1, and P3, respectively. Next, overlaying the structure of SARS-CoV M^{pro} + **ML188 (R)** (PDB: 3V3M) and SARS-CoV-2 M^{pro} + **GC376** (PDB: 6WTT) suggested that the *tert*-butyl at the P3 substitution of **ML188 (R)** can be extended to fit in the S4 pocket (Figure 3B, D). Previous structure–activity relationship studies of **GC376** indicate that P4 substitution is important, while P3 substitution does not contribute significantly to the binding affinity, as it is solvent exposed.[3,8,9,16] Similarly, the overlaying structures of SARS-CoV M^{pro} + **ML188 (R)** (PDB: 3V3M) and SARS-CoV-2 M^{pro} + **UAWJ247** (PDB: 6XBH) suggested that the 4-*tert*-butyl at the P2 substitution of **ML188 (R)** can be replaced by phenyl to occupy the extra space in the S2 pocket (Figure 3C, D). Overall, binding site analysis suggests that extending the P2 and P3 substitutions of **ML188 (R)** might lead to better shape complementarity with the SARS-CoV-2 M^{pro} (Figure 3E). In practice, we adopted a stepwise optimization procedure in which the P3 and P2 substitutions were optimized individually in step 1 and then the optimal P2/P3 substitutions were combined in step 2 (Figure 3E).

Guided by the design rationale elucidated above, a focused library of **ML188** analogs was designed and synthesized (Figure 4). As the P1′ furyl and P1 pyridinyl both form a critical hydrogen bond with the M^{pro} (Figure 4A, B), the P1′ and P1 substitutions were kept with minimal variations for the design of noncovalent inhibitors (Figure 4C). All designed compounds were synthesized using the one pot Ugi four-component reaction and tested as enantiomer/diastereomer mixtures (Figure 4C). To circumvent the need of relying on an expensive chiral HPLC column for the separation of

https://doi.org/10.1021/acs.jmedchem.1c00509
J. Med. Chem. 2022, 65, 2848–2865

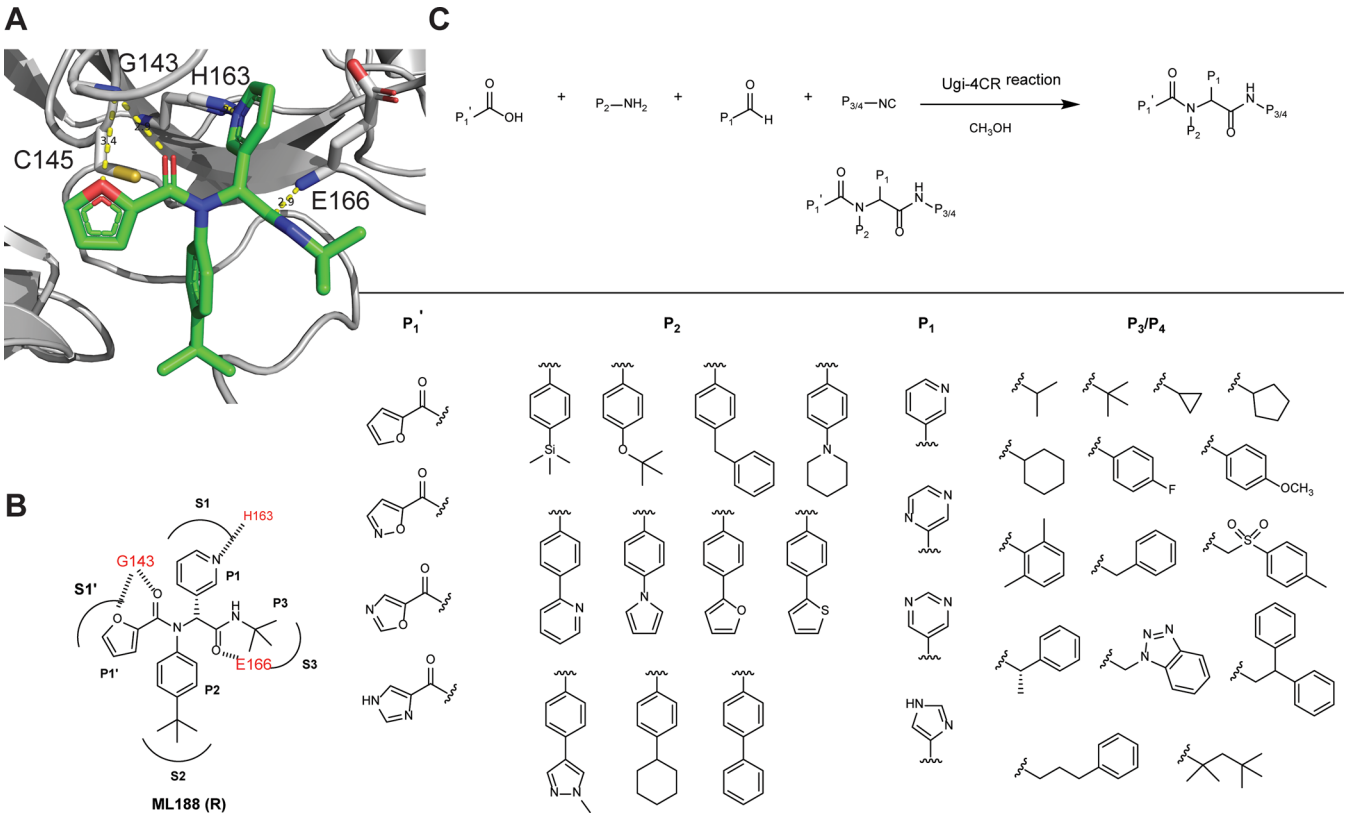

Figure 4. Design and synthesis of a focused library of noncovalent SARS-CoV-2 M^{pro} inhibitors. (A) X-ray crystal structure of SARS-CoV M^{pro} + **ML188 (R)** (PDB: 3V3M). (B) Binding interactions of **ML188 (R)** with SARS-CoV M^{pro}. (C) Synthesis of **ML188** analogs using the Ugi four-component reaction.

enantiomers, we strategically introduced the chiral isocyanide so that the diastereomer product mixture can be separated by convenient silica gel column or reverse phase HPLC column purification.[17]

Structure−Activity Relationship Studies of Noncovalent SARS-CoV-2 M^{pro} Inhibitors. In total, 39 compounds were synthesized (Figure 5A−E) and all compounds were initially tested as a mixture of enantiomers or diastereomers in the FRET-based enzymatic assay against SARS-CoV-2 M^{pro} at 20 μM (Figure 5F). Compounds showing more than 50% inhibition at 20 μM were further titrated to determine the IC_{50} values. Next, compounds with IC_{50} values lower than 5 μM were selected for cellular cytotoxicity profiling in Vero E6 cells, the cell line which was used for the SARS-CoV-2 antiviral assay. The purpose was to prioritize lead candidates for the *in vitro* cellular antiviral assay with infectious SARS-CoV-2. As shown in Figure 5, the majority of the designed compounds showed more than 50% inhibition when tested at 20 μM. Specifically, Figure 5A lists compounds with P4 variations. As a reference, **ML188** (**1**) (racemic mixture) inhibits SARS-CoV-2 M^{pro} with an IC_{50} value of 10.96 ± 1.58 μM. It was found that compounds **2**, **3**, **5**, **6**, **7**, **8**, **10**, and **13** had improved enzymatic inhibition compared to **ML188** (**1**). These results suggest that (a) isopropyl (**2**), cyclopropyl (**3**), cyclopentyl (**5**), cyclohexyl (**6**), and phenyl (**7** and **8**) are the more favorable substitutions at the P3 position than *tert*-butyl and (b) compound **13** with the (*S*)-α-methylbenzyl substitution at the P3 position had improved potency, which suggests that extending the substitutions to the S4 pocket might improve the enzymatic inhibition (Figure 3B). Given the advantage of convenient separation of diastereomers over enantiomers, we therefore decided to fix the P3/P4 substitution as α-methylbenzyl substitution during the P2 optimization (Figure 5B). All compounds in Figure 5B were designed to have extended substitutions at the 4-position of benzyl to occupy the extra space in the S2 pocket (Figure 3C). Consistent with the design hypothesis, several compounds including **14**, **17**, **18**, **19**, **20**, **21**, and **23** had significantly improved enzymatic inhibition (IC_{50} < 3 μM) compared to compound **13**. Replacing the *tert*-butyl in compound **13** with the bulkier trimethylsilyl led to compound **14** with a 2.9-fold increase in M^{pro} inhibition. Cyclohexyl (**17**), thienyl (**19**), pyrrolyl (**20**), pyridinyl (**21**), and phenyl (**23**) were found to be the most favorable substitutions at the S2 pocket. Compound **16** with piperidyl substitution had similar potency as compound **13**, while compound **15** with O-*tert* butyl was less active. Further extending the substitution to benzyl led to compound **22** that was inactive, suggesting biphenyl might be the longest substitution that can be accommodated at the S2 pocket.

The P1′ and P1 substitutions (Figure 5C, D) were chosen to retain the critical hydrogen bonds in **ML188** (Figure 4A). It was found that imidazole (**24**) was tolerated at the P1′ position (IC_{50} = 0.96 ± 0.09 μM), followed by isoxazole (**25**) (IC_{50} = 2.47 ± 0.27 μM) and oxazole (**26**) (IC_{50} = 4.97 ± 0.78 μM). Pyrazine (**27**) was tolerated at the P1 position (IC_{50} = 4.93 ± 0.79 μM); however, imidazole (**28**) and pyrimidine (**29**) were not preferred (IC_{50} > 20 μM).

Next, the above identified favorable P1′, P2, P1, and P3/P4 substitutions were combined and the designed compounds were shown in Figure 5E. Compounds **36**, **37**, and **38** were the most potent leads with IC_{50} values of 0.81 ± 0.24, 0.67 ± 0.15,

https://doi.org/10.1021/acs.jmedchem.1c00509
J. Med. Chem. 2022, 65, 2848−2865

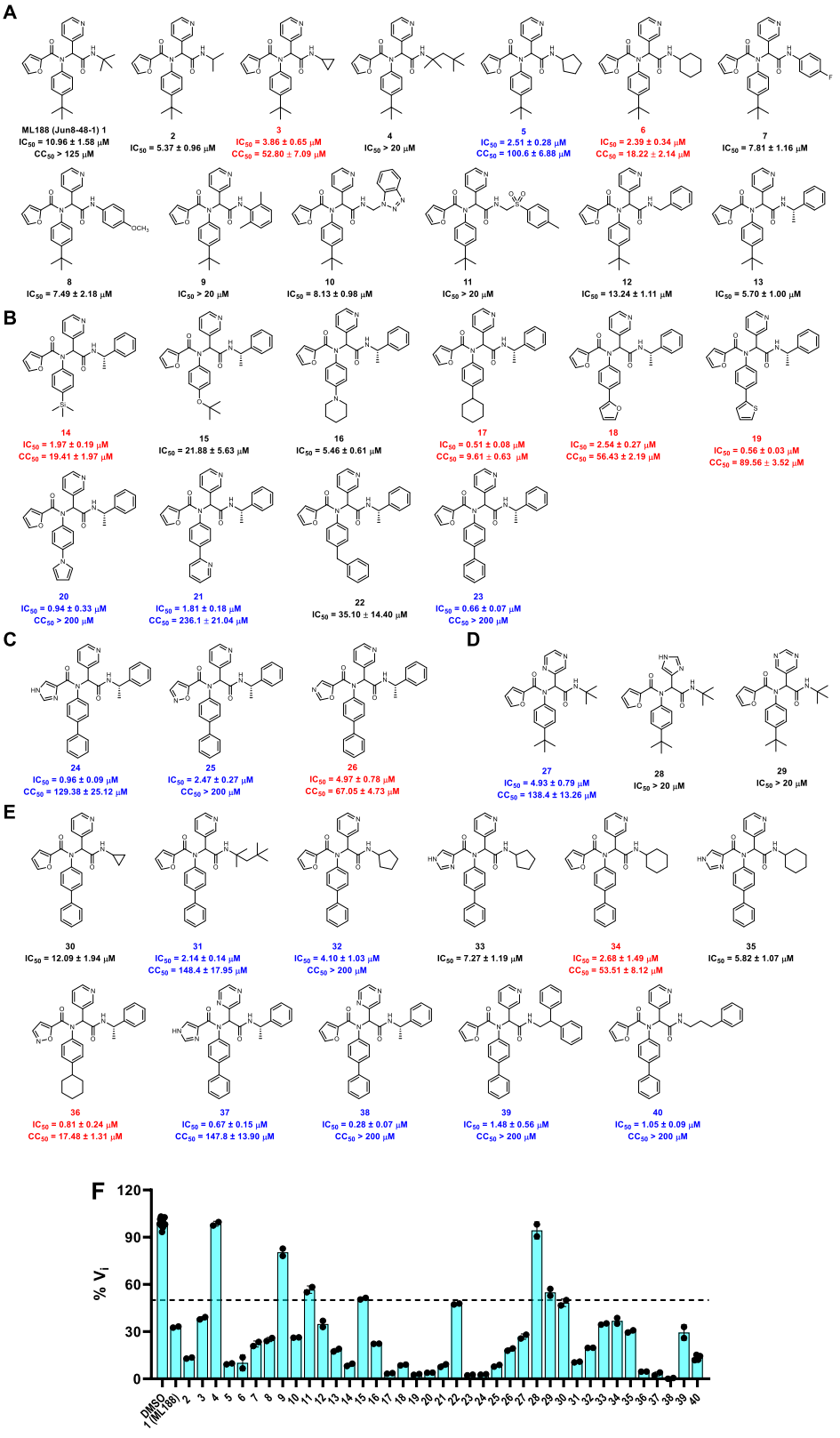

Figure 5. Structures of noncovalent and covalent SARS-CoV-2 M^{pro} inhibitors and the enzymatic inhibition against SARS-CoV-2 M^{pro}. (A) Noncovalent analogs with P3/P4 modifications. (B) Noncovalent analogs with P2 modifications. (C) Noncovalent analogs with P1′ modifications. (D) Noncovalent analogs with P1 modifications. (E) Noncovalent analogs with combined P1′, P1, P2, and P3/P4 modifications. Compounds with potent enzymatic inhibition (IC_{50} < 5 μM) but moderate to high cellular cytotoxicity (CC_{50} < 100 μM) are labeled in red. Compounds with both potent enzymatic inhibition (IC_{50} < 5 μM) and low cellular cytotoxicity (CC_{50} > 100 μM) are labeled in blue. (F) Percentage enzymatic activity of SARS-CoV-2 M^{pro} in the presence of the designed compounds at 20 μM concentration.

https://doi.org/10.1021/acs.jmedchem.1c00509
J. Med. Chem. 2022, 65, 2848−2865

A

Compound ID	SARS-CoV-2 M^{pro} IC_{50} (μM)	SARS-CoV M^{pro} IC_{50} (μM)	SARS-CoV-2 PL^{pro} IC_{50} (μM)	Vero E6 Cytotoxicity CC_{50} (μM)	SARS-CoV-2 antiviral assay EC_{50} (μM)	Selectivity index SI CC_{50}/EC_{50}
ML188 (1)	10.96 ± 1.58	11.23 ± 1.61	> 60	> 125	>20	N.A.
GC376	0.033 ± 0.003	0.035 ± 0.002	> 60	> 125	1.51 ± 0.27	> 82.8
20	0.94 ± 0.33	N.T.	N.T.	> 200	1.73 ± 0.19	> 115.6
23	0.66 ± 0.07	N.T.	N.T.	> 200	1.61 ± 0.29	> 124.2
24	0.96 ± 0.09	N.T.	N.T.	129.38 ± 25.12	13.06 ± 2.30	9.9
37	0.67 ± 0.15	N.T.	N.T.	147.8 ± 13.9	4.54 ± 0.69	32.6
38	0.28 ± 0.07	N.T.	N.T.	> 200	0.82 ± 0.56	> 243.9
40	1.05 ± 0.09	N.T.	N.T.	> 200	2.04 ± 1.08	> 98.0
23R	0.20 ± 0.01	0.27 ± 0.03	> 60	> 100	1.27 ± 0.09	> 78.7
23S	> 20	N.T.	N. T.	N.T.	N.T.	N.A.

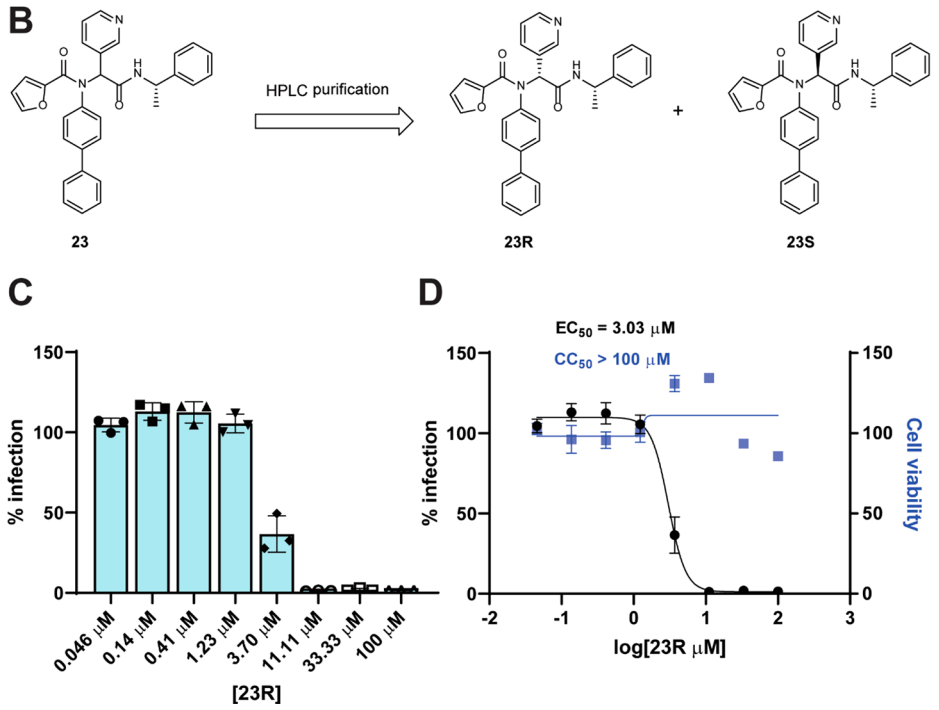

Figure 6. Enzymatic inhibition, cellular antiviral activity, and selectivity index of noncovalent M^{pro} inhibitors. (A) Antiviral activity and selectivity index of noncovalent SARS-CoV-2 M^{pro} inhibitors. (Selection criteria IC_{50} < 1 μM, CC_{50} > 100 μM). Antiviral assay was performed using the SARS-CoV-2 USA-WA1/2020 isolate in Vero E6 cells with an MOI of 0.05. (B) Chemical structures of the two diastereomers **23R** and **23S**. The absolute stereochemistry of compound **23R** was determined in the cocrystal structure of this diastereomer with SARS-CoV-2 M^{pro} (PDB: 7KX5). (C and D) Antiviral activity of **23R** against SARS-CoV-2 in Calu-3 cells. (C) Raw data of the percentage of immunofluorescence positive cells with different concentrations of **23R**. (D) Antiviral potency and cytotoxicity plots. N.T. = not tested. N.A. = not applicable.

and 0.28 ± 0.07 μM, respectively. Compounds **39** and **40** were also highly active with IC_{50} values of 1.48 ± 0.56 and 1.05 ± 0.09 μM, respectively.

Among the active compounds with IC_{50} values lower than 5 μM, compounds **3**, **6**, **14**, **17**, **18**, **19**, **26**, **34**, and **36** had moderate to high cellular cytotoxicity in Vero E6 cells (Figure 5A–E red), while compounds **5**, **20**, **21**, **23**, **24**, **25**, **27**, **31**, **32**, **37**, **38**, **39**, and **40** were well tolerated and the CC_{50} values were greater than 100 μM (Figure 5A–E blue).

Cellular Antiviral Activity of Noncovalent SARS-CoV-2 M^{pro} Inhibitors. Next, compounds with potent enzymatic inhibition ($IC_{50} \leq 1$ μM) and low cellular cytotoxicity (CC_{50} > 100 μM) were prioritized for the cellular antiviral assay with infectious SARS-CoV-2 in Vero E6 cells using the immunofluorescence assay as the primary assay (Figure 6A). **ML188** (**1**) was included as a control. It was found that **ML188** (**1**) was inactive in the antiviral assay (EC_{50} > 20 μM), probably due to its incomplete inhibition of the M^{pro} in the cellular content. Gratifyingly, compounds **20**, **23**, **37**, **38**, and **40** all had potent cellular antiviral activity with EC_{50} values ranging from 0.82 to 4.54 μM. Compound **24** was less active (EC_{50} = 13.06 ± 2.30 μM), possibly due to the poor cellular membrane permeability.

Given the potent antiviral activity and high selectivity index of these potent lead compounds, we then selected the noncovalent inhibitor **23** for further characterization. The two diastereomers of **23** were separated by reverse phase HPLC (Figure 6B). Both diastereomers were tested in the FRET-based enzymatic assay. **GC376** was included as a positive control. It was found that **23R** is the active diastereomer with an IC_{50} value of 0.20 ± 0.01 μM, while the **23S** diastereomer was not active (IC_{50} > 20 μM) (Figure

https://doi.org/10.1021/acs.jmedchem.1c00509
J. Med. Chem. 2022, 65, 2848–2865

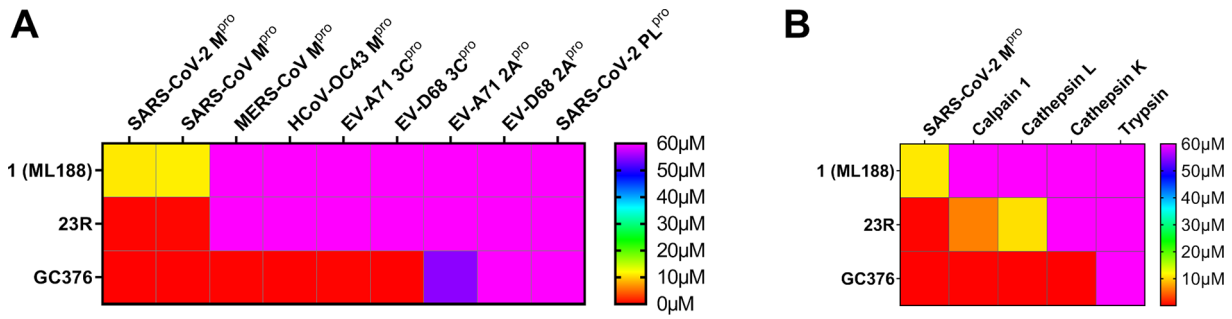

Figure 7. Selectivity of noncovalent and covalent SARS-CoV-2 M^{pro} inhibitors shown in a color map. (A) Selectivity against viral cysteine proteases. (B) Selectivity against host proteases. The values plotted were the IC_{50} values from the FRET-based enzymatic assay.

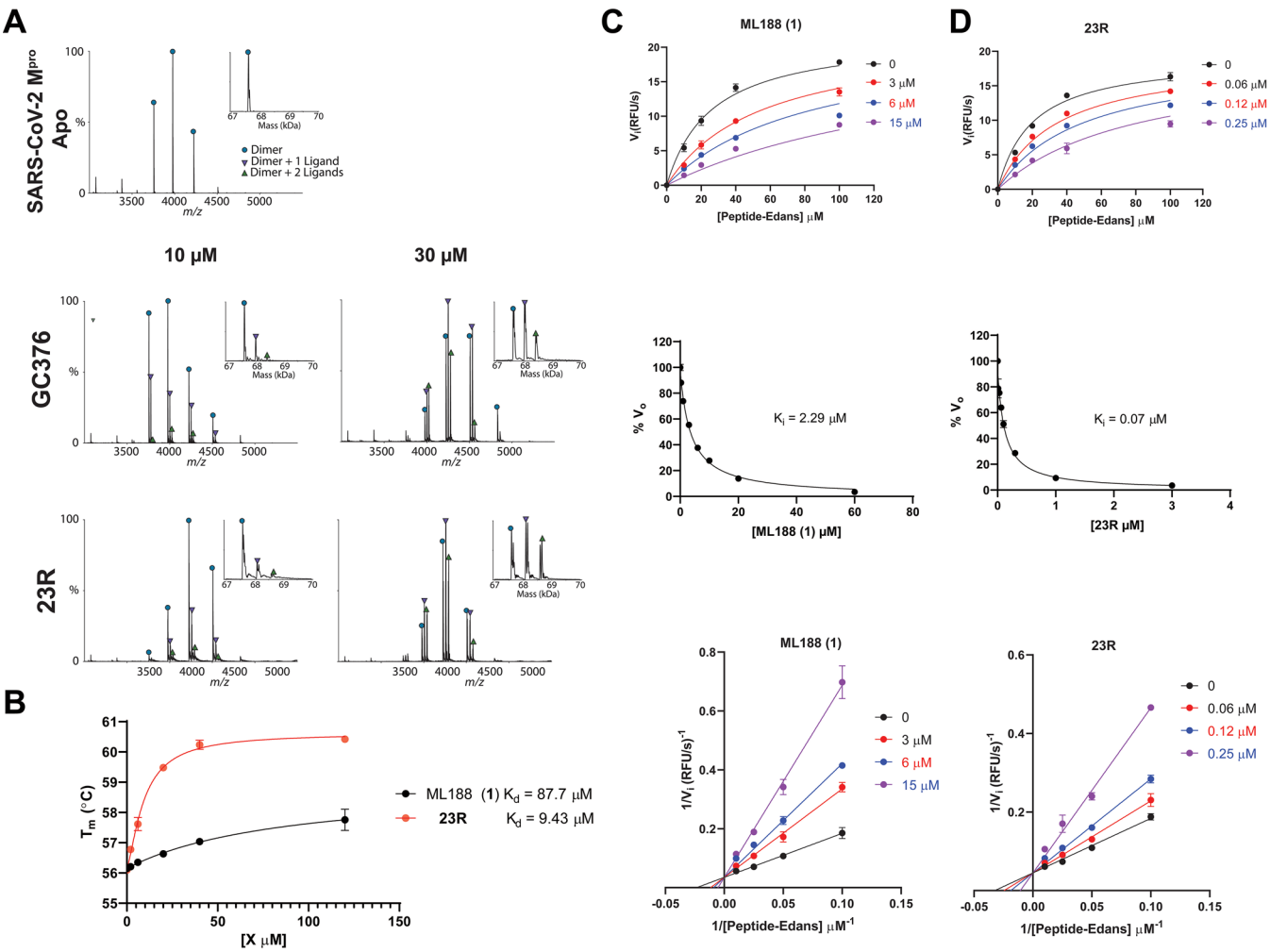

Figure 8. Characterization of the mechanism of action of **23R** to SARS-CoV-2 M^{pro} using native mass spectrometry, thermal shift assay, and enzyme kinetic studies. (A) Binding of **23R** to SARS-CoV-2 M^{pro} using native mass spectrometry. Native mass spectra with the inset deconvolved spectra revealing ligand binding with 10 μM or 30 μM **GC376** added (middle panel) and 10 μM and 30 μM **23R** (bottom panel) with 4 mM DTT added. The peaks are annotated with the blue circle as the dimer, the green down triangle as the dimer with one ligand bound, and the purple up triangle as the dimer with two ligands bound. (B) Dose-dependent melting temperature (T_m) shift in the thermal shift assay. 3 μM SARS-CoV-2 M^{pro} protein was incubated with various concentrations of ML188 or **23R** in the presence of 4 mM DTT. Measured T_m was plotted against compound concentration with one-site binding function in Prism 8. (C and D) Enzymatic kinetic assay with **ML188** and compound **23R**. Kinetic parameters in the presence of various concentrations of **ML188** or **23R** were globally fitted with a Michaelis−Menten function in prism 8 (top panels); double-reciprocal plots are shown in the right panels. The middle panels show the Morrison plots of compounds **ML188** and **23R** with 20 μM FRET substrate used.

6A). The stereochemistry of **23R** was determined by the cocrystal structure with SARS-CoV-2 M^{pro} as described in the following section. Compared with the parent compound **ML188** (**1**), the optimized lead **23R** had more than a 54-fold increase in enzymatic inhibition against SARS-CoV-2 M^{pro}. Compound **23R** also showed comparable potency against SARS-CoV M^{pro} with an IC_{50} value of 0.27 ± 0.03 μM. Neither **ML188** (**1**) nor **23R** inhibited the SARS-CoV-2

https://doi.org/10.1021/acs.jmedchem.1c00509
J. Med. Chem. 2022, 65, 2848−2865

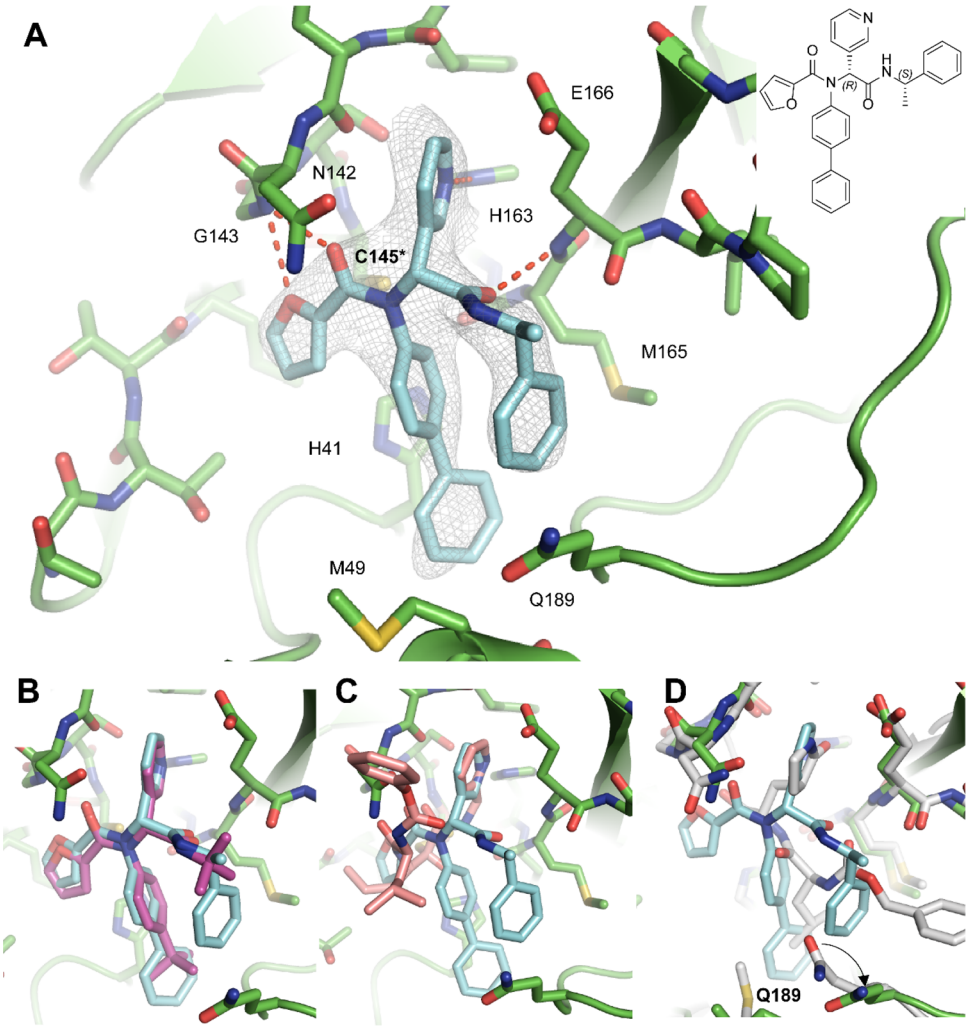

Figure 9. X-ray crystal structure of SARS-CoV-2 M^{pro} in complex with **23R**. (A) X-ray crystal structure of SARS-CoV-2 M^{pro} in complex with **23R** (PDB: 7KX5). (B) Superimposed structures of SARS-CoV-2 M^{pro} + **23R** (PDB: 7KX5) and SARS-CoV M^{pro} + **ML188 (R)** (PDB: 3V3M). (C) Superimposed structures of SARS-CoV-2 M^{pro} + **23R** (PDB: 7KX5) and SARS-CoV-2 M^{pro} + **calpain inhibitor XII** (PDB: 6XFN). (D) Superimposed structures of SARS-CoV-2 M^{pro} + **23R** (PDB: 7KX5) and SARS-CoV-2 M^{pro} + **GC376** (PDB: 6WTT).

papain-like protease (PL^{pro}) (IC_{50} > 20 μM) (Figure 6A), suggesting the inhibition of SARS-CoV-2 M^{pro} by **23R** is specific.

Next, the antiviral activity of **23R** was tested against SARS-CoV-2 (USA-WA1/2020 isolate) in Vero E6 cells using the immunofluorescence assay. It was found that compound **23R** had an EC_{50} value of 1.27 μM (Figure 6A), which was similar to the antiviral potency of the covalent inhibitor **GC376** (EC_{50} = 1.51 μM). Compound **23R** was also not cytotoxic to Vero E6 cells at up to 100 μM. In contrast, the parent compound **ML188** (**1**) had no detectable antiviral activity when tested at up to 20 μM. To further confirm the antiviral activity of compound **23R**, we performed a secondary antiviral assay in the human lung epithelial Calu-3 cell line, which endogenously expresses TMPRSS2 and is widely used as a physiological relevant cell line for SARS-CoV-2 infection. It was found that compound **23R** inhibited SARS-CoV-2 (USA-WA1/2020 isolate) replication in Calu-3 cells with an EC_{50} value of 3.03 μM, and it was not cytotoxic at up to 100 μM (Figure 6C, D).

Profiling the Target Selectivity of 23R against Other Viral Cysteine Proteases and Host Proteases. One of the major challenges facing cysteine protease inhibitors is the target selectivity.[18,19] It was recently reported that **GC376** inhibits host cathepsins B and L in addition to SARS-CoV-2 M^{pro},[20] and **GC376** analogs **compound_1** and **zyy16** that contained the aldehyde and cyanohydrin warheads, respectively, inhibit both calpain 1 and cathepsin K.[21] These results raised the concern of the selectivity of this class of covalent inhibitors. To profile the target selectivity of the lead compounds developed in this study, we selected compound **23R** as a representative example of the noncovalent inhibitor. **ML188** (**1**) and **GC376** were included as controls. The compounds were tested against a panel of viral cysteine proteases including SARS-CoV M^{pro}, MERS-CoV M^{pro}, HCoV-OC43 M^{pro}, EV-A71 $3C^{pro}$, EV-D68 $3C^{pro}$, EV-A71 $2A^{pro}$, EV-D68 $2A^{pro}$, and SARS-CoV-2 PL^{pro}, as well as host cysteine proteases calpain 1, cathepsin K, cathepsin L, and serine protease trypsin. It was found that **GC376** inhibited all the M^{pro} and $3C^{pro}$ tested including SARS-CoV-2 M^{pro}, SARS-CoV M^{pro}, MERS-CoV M^{pro}, HCoV-OC43 M^{pro}, EV-A71 $3C^{pro}$, and EV-D68 $3C^{pro}$ ($IC_{50} \leq 0.16$ μM), but not the unrelated EV-A71 $2A^{pro}$, EV-D68 $2A^{pro}$, and SARS-CoV-2 PL^{pro} (IC_{50} > 50 μM) (Figure 7A and Table S1). In addition, **GC376** also inhibited host cysteine proteases calpain 1,

https://doi.org/10.1021/acs.jmedchem.1c00509
J. Med. Chem. 2022, 65, 2848−2865

cathepsin K, and cathepsin L ($IC_{50} \leq 0.074$ μM) but not the serine protease trypsin ($IC_{50} > 50$ μM) (Figure 7B and Table S1). In contrast, the noncovalent inhibitor **23R** developed in this study only selectively inhibited SARS-CoV-2 M^{pro} and SARS-CoV M^{pro} with high potency ($IC_{50} \leq 0.27$ μM) but not other viral proteases tested, which was similar to **ML188 (1)** (Figure 7A and Table S1). Compound **23R** showed weak inhibition against calpain 1 and cathepsin L with IC_{50} values of 6.00 μM and 10.5 μM, respectively, corresponding to selectivity indexes of 40 and 70 with regard to SARS-CoV-2 M^{pro} inhibition (Figure 7B and Table S1).

Mechanism of Action of Noncovalent Inhibitor 23R in Inhibiting SARS-CoV-2 M^{pro}. The mechanism of action was characterized using native mass spectrometry, the thermal shift-binding assay, and enzymatic kinetic studies (Figure 8). In the native mass spectrometry binding assay, compound **23R** showed dose-dependent binding to SARS-CoV-2 M^{pro}, similar to the positive control **GC376**, with a binding stoichiometry of one drug per monomer (Figure 8A). Similarly, compound **23R** showed dose-dependent stabilization of the SARS-CoV-2 M^{pro} in the thermal shift binding assay with an apparent K_d value of 9.43 μM, a 9.3-fold decrease compared to **ML188 (1)** (Figure 8B). In the enzymatic kinetic studies, **23R** was shown to be a noncovalent inhibitor with a K_i value of 0.07 μM (Figure 8C, D top and middle panels). In comparison, the K_i for the parent compound **ML188 (1)** is 2.29 μM. The Lineweaver−Burk or double-reciprocal plot with different compound concentrations yielded an intercept at the *Y*-axis, suggesting that **23R** is a competitive inhibitor similar to **ML188 (1)** (Figure 8C, D bottom panel). Overall, the enzymatic kinetic studies confirmed that compound **23R** is a noncovalent inhibitor of SARS-CoV-2 M^{pro}.

X-ray Crystal Structure of SARS-CoV-2 M^{pro} with 23R. Using X-ray crystallography, we successfully determined the binding pose of **23R** with SARS-CoV-2 M^{pro} at 2.6 Å resolution (Figure 9A, Table S2). Electron density reveals the body of **23R** extends throughout the substrate binding channel, with side chains occupying S1′, S1, S2, and a previously unexplored subpocket in between S2 and S4. The binding pose is similar to the previously solved structure of SARS-CoV M^{pro} with **ML188 (R)** (PDB: 3V3M),[13] consistent with the similarities between the two compounds and between the two proteins (Figure 9B). The furyl moiety of **23R** binds to a portion of the P1′ site, which normally accommodates small hydrophobic residues. While the furylamide carbonyl group of **23R** does not insert into the oxyanion hole, it does form a bifurcated hydrogen bond with the apical residue of this oxyanion hole, Gly143. However, the furan ring oxygen is likely a weaker hydrogen bond acceptor than the amide oxygen, and it lies outside of the plane of Gly143's amide NH. Directly attached to the furylamide moiety is a P2 biphenyl group and a P1 pyridinyl ring. The P2 biphenyl group projects directly into the S2 pocket, which prefers hydrophobic residues such as leucine and phenylalanine. As expected, the P1 pyridinyl ring occupies the S1 pocket, which is known for its strict preference for glutamine. While most M^{pro} inhibitors bear a pyrrolidinone glutamine mimetic at the P1 position, we determined that more hydrophobic residues can also bind to the S1 site and that hydrogen bond formation with His163 is critical for inhibition.[8] In this instance, the pyridinyl ring of **23R** is nearly superimposable with the same moiety from **calpain inhibitor XII** (Figure 9C) forming a close (2.9 Å) hydrogen bond with His163. An amide bond connecting the pyridinyl ring to the α-methylbenzyl moiety forms a hydrogen bond with the main chain of Glu166. The benzyl ring of the α-methylbenzyl moiety is partially positioned in both the S2 and S4 pockets, a novel binding pose that has not been observed with existing M^{pro} inhibitors. Normally, a substituent at this position would be expected to flip away from the enzyme core toward the solvent-exposed S3 pocket, which explains why P3 substitutions have little to no influence on the enzymatic inhibition.[4] However, the chirality and hydrophobic nature of the benzyl ring in **23R** cause it to project toward the core near the S2 pocket, forcing Gln189 to rotate outward (Figure 9D). This conformation is reinforced by π-stacking interactions with the first phenyl of the biphenyl substituent. Notably, the binding pose of **23R** features continuous intramolecular π-stacking, where the phenyl is sandwiched by furan and benzyl groups, potentially contributing to its potent inhibition of M^{pro}. Meanwhile, the S4 pocket remains largely unoccupied by **23R**, leaving room for further improvement. In summary, the X-ray crystal structure of SARS-CoV-2 M^{pro} in complex with **23R** revealed two interesting structural features: (1) The P2 biphenyl is probably the longest substitution that can be accommodated in the S2 pocket, which is consistent with our design hypothesis. (2) The benzyl group from the terminal α-methylbenzyl fits in a pocket in between the S2 and S4 pockets, and this is a ligand-induced binding site that has not been previously explored. Although this is unexpected from the design perspective, this novel binding mode suggests that the new binding pocket in between S2 and S4 can be explored for inhibitor design.

CONCLUSION

The viral M^{pro} is a high profile antiviral drug target, and several M^{pro} inhibitors are now in animal model studies and human clinical trials.[6] Among the known M^{pro} inhibitors, the majority are covalent inhibitors such as **GC376** analogs that contain a pyrrolidone in the P1 position as a glutamine mimetic. Several structurally distinct compounds including ebselen, disulfiram, carmofur, PX-12, tideglusib, and shiknonin were claimed as M^{pro} inhibitors[22,23] but were later proved to be promiscuous nonspecific cysteine protease inhibitors.[24,25] In addition, noncovalent inhibitors such as **ML188 (R)** were developed and validated as SARS-CoV M^{pro} inhibitors.[5,13] Several follow up studies have been conducted to optimize the enzymatic potency of this series of compounds against SARS-CoV M^{pro} and SARS-CoV-2 M^{pro}. However, no significant improvement has been made, and **ML188 (R)** remains the only noncovalent inhibitor with moderate antiviral activity against SARS-CoV ($EC_{50} = 12.9 \pm 0.7$ μM).[14,15] Nevertheless, given the sequence and structural similarities between SARS-CoV and SARS-CoV-2 M^{pro}, and the similar binding mode of **ML188 (R)** and **calpain inhibitor XII**, we hypothesize that **ML188 (R)** is a promising scaffold for structure-based drug design. In this study, we developed an expedited drug discovery approach for the design of noncovalent SARS-CoV-2 M^{pro} inhibitors. The design approach couples the superimposed X-ray crystal structures with the one-pot Ugi 4CR synthetic methodology. We were able to improve the enzymatic inhibition potency of **ML188 (1)** by 54-fold from a focused library of 39 noncovalent inhibitors. This is a significant advantage compared to covalent inhibitors such as **GC376**, which involves at least a five-step synthesis. In addition, by introducing the chiral isocyanide, the diastereomer product can be conveniently separated by either silica gel column or

https://doi.org/10.1021/acs.jmedchem.1c00509
J. Med. Chem. 2022, 65, 2848−2865

reverse phase HPLC column, bypassing the need for an expensive chiral HPLC column. Target selectivity profiling showed that the noncovalent inhibitor **23R** only selectively inhibits SARS-CoV-2 and SARS-CoV M^{pro}, but not other viral proteases and host proteases including calpain 1, cathepsins L and K, and trypsin. In contrast, the covalent M^{pro} inhibitor **GC376** is not selective and inhibits host cysteine proteases, which might result in potential side effects. Furthermore, the X-ray crystal structure of SARS-CoV-2 M^{pro} in complex with **23R** reveals a ligand-induced binding pocket in between S2 and S4 sites that can be explored for drug design. Overall, using the expedited drug discovery approach, this study revealed a promising noncovalent M^{pro} inhibitor **23R** with a well characterized mechanism of action and potent cellular antiviral activity for further development.

MATERIALS AND METHODS

Cell Lines and Viruses. VERO E6 cells (ATCC, CRL-1586) were cultured in Dulbecco's modified Eagle's medium (DMEM), supplemented with 5% heat inactivated FBS in a 37 °C incubator with 5% CO_2. SARS-CoV-2, isolate USA-WA1/2020 (NR-52281), was obtained through BEI Resources and propagated once on VERO E6 cells before it was used for this study. Studies involving SARS-CoV-2 were performed at the UTHSCSA biosafety level-3 laboratory by personnel wearing powered air purifying respirators.

Protein Expression and Purification. SARS CoV-2 main protease (M^{pro} or 3CL) gene from strain BetaCoV/Wuhan/WIV04/2019 and SARS-CoV main protease from strain CDC#200301157 in the pET29a(+) vector with *E. coli* codon optimization were ordered from GenScript (Piscataway, NJ). The M^{pro} gene was then subcloned into pE-SUMO vector as described previously.[7,8] The expression and purification of SARS-CoV and SARS-CoV-2 M^{pro} with unmodified N- and C-termini were detailed in our previous publication.[8]

The expression and purification of SARS CoV-2 papain-like protease (PL^{pro}) were also described in our previous publications.[7,8,24]

The expression and purification of EV-A71 $2A^{pro}$ and $3C^{pro}$, EV-D68 $2A^{pro}$ and $3C^{pro}$ were described in our previous publications.[24,26]

Cathepsin K and Cathepsin L were purchased from EMD Millipore (catalog #. 219461 and 219402, respectively).

Calpain 1 and trypsin were purchased from Sigma-Aldrich (catalog #. C6108 and T6763, respectively).

Peptide Synthesis. The SARS-CoV-2 M^{pro} FRET substrate Dabcyl-KTSAVLQ/SGFRKME(Edans) was synthesized as described before.[7] The SARS-CoV-2 PL^{pro}, EV-A71 $2A^{pro}$ and $3C^{pro}$, and EV-D68 $2A^{pro}$ and $3C^{pro}$ FRET substrates were listed in our previous publication[24] and were synthesized by solid-phase synthesis through iterative cycles of coupling and deprotection using the previously optimized procedure.[27]

General Chemical Methods. All chemicals were purchased from commercial vendors and used without further purification unless otherwise noted. ^1H and ^{13}C NMR spectra were recorded on a Bruker-400 or -500 NMR spectrometer. Chemical shifts are reported in parts per million referenced with respect to residual solvent (CD_3OD) 3.31 ppm, (DMSO-d_6) 2.50 ppm, and ($CDCl_3$) 7.26 ppm or from internal standard tetramethylsilane (TMS) 0.00 ppm. The following abbreviations were used in reporting spectra: s, singlet; d, doublet; t, triplet; q, quartet; m, multiplet; dd, doublet of doublets; ddd, doublet of doublet of doublets. All reactions were carried out under N_2 atmosphere, unless otherwise stated. HPLC-grade solvents were used for all reactions. Flash column chromatography was performed using silica gel (230−400 mesh, Merck). High resolution mass spectra were obtained using an OrbitrapTM for all the compounds, obtained in an Ion Cyclotron Resonance (ICR) spectrometer. The purity was assessed by using Shimadzu UPLC with Shimdazu C18-AQ column (4.6 × 150 mm P/N #227-30767-05) at a flow rate of 1 mL/min; λ = 254 and 220 nm; mobile phase A, 0.1% trifluoroacetic acid in H_2O, and mobile phase B, 0.1% trifluoroacetic acid in 90% CH_3CN and 10% H_2O. The gradients are 0−2 min 10% B, 2−15 min 10%−100% B, 15−18 min, 100% B, 18.1−20 min 10% B. All compounds submitted for testing were confirmed to be >95.0% purity by HPLC traces. All final products were characterized by proton and carbon NMR, HPLC, and HRMS.

General Procedure for Ugi-4CR Reaction.

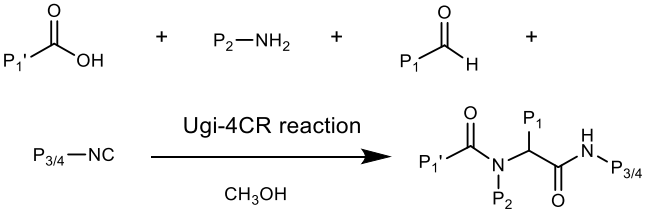

Ug-4CR reaction was performed according to the reported procedure with modifications.[13] Amine (1.0 equiv) and aldehyde (1.0 equiv) were mixed in methanol (10 mL) and stirred at room temperature for 30 min. Then carboxylic acid (1.0 equiv) and isocyanide (1.0 equiv) were added sequentially and the resulting mixture was stirred at room temperature overnight. After that, the solvent was removed under reduced pressure and the crude product was purified with flash silica gel chromatography (methanol in dichloromethane 1−5% or acetone in hexane 30−80%).

*General Procedures for the Synthesis of Compounds **24, 28, 33, 35, and 37** by TFA Deprotection.* To a solution of N-trityl-protected Ugi-4CR compound in dichloromethane (5 mL) was added TFA (1 mL). The mixture was stirred at room temperature for 2 h, and the solvent was removed under reduced pressure. The crude mixture was diluted in dichloromethane and purified by silica gel flash column chromatography (ammonia 10% methanol in dichloromethane 10−15%) to give the final product.

*Procedure for the Synthesis of Compound **18** by Suzuki−Miyamura Cross-coupling.*

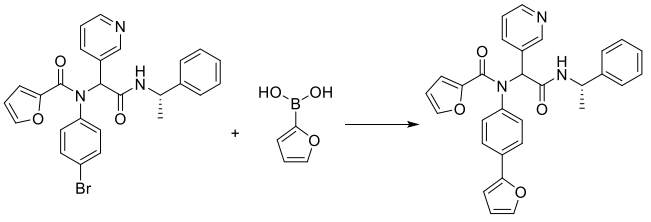

18

To solution of 2-[N-(4-bromophenyl)-1-(furan-2-yl)formamido]-N-[(1S)-1-phenylethyl]-2-(pyridin-3-yl)acetamide (1 mmol) and furan-2-boronic acid (1 mmol) in 1,4-dioxane in a microwave reaction vial was added an aqueous solution of K_2CO_3 (4 mmol). The resulting solution was purged with N_2 for 5 min. The catalyst, $Pd(PPh_3)_4$ (0.1 mmol), was added in one portion. The vial was capped and heated to 140 °C for 30 min with microwave irradiation. After cooling down to room temperature, the reaction solution was diluted with dichloromethane and extracted with water, followed by brine. The organic layer was dried over $MgSO_4$, filtrated, and concentrated under reduced pressure. The crude product was purified by silica gel flash column chromatography (methanol in dichloromethane 1−5%) to give the final product.

Procedure for the Synthesis of 4-(Thiophen-2-yl)aniline by Suzuki−Miyamura Cross-coupling.

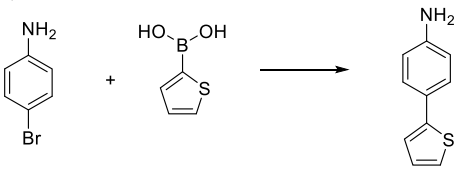

The starting material 4-(thiophen-2-yl)aniline used for the synthesis of compound **19** was prepared using the following procedure. To a suspension of thiophene-2-boronic acid (1.0 mmol) and sodium carbonate (1.0 mmol) in toluene/methanol (4:1, 40 mL) was added 4-bromoaniline (1.0 mmol). The resulting solution was purged with

https://doi.org/10.1021/acs.jmedchem.1c00509
J. Med. Chem. 2022, 65, 2848−2865

N_2 for 10 min. The catalyst, $Pd(PPh_3)_4$ (0.1 mmol), was added in one portion. The reaction mixture was stirred for 16 h at 100 °C. After cooling to room temperature, the reaction mixture was diluted with ethyl acetate (100 mL) and washed with water (100 mL). The organic layer was dried over $MgSO_4$, filtrated, and concentrated under reduced pressure. The crude product was purified by silica gel flash column chromatography (ethyl acetate in hexane 20−40%) to give the final product.

4-(Thiophen-2-yl)aniline. White solid. 31% yield. ^{1}H NMR (500 MHz, $CDCl_3$) δ 7.43−7.38 (m, 2H), 7.17−7.12 (m, 2H), 7.01 (dd, J = 5.0, 3.6 Hz, 1H), 6.69−6.63 (m, 2H), 3.68 (s, 2H). ^{13}C NMR (126 MHz, $CDCl_3$) δ 146.10, 145.11, 127.93, 127.25, 125.24, 123.17, 121.36, 115.39.

The isocyanide used for the synthesis of compound **40** was prepared and used in the method below:

Procedure for Synthesis of N-(3-Phenylpropyl)formamide.

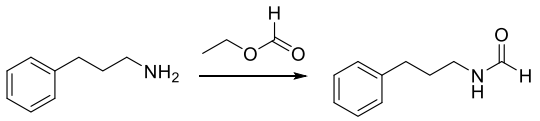

3-Phenyl propylamine (2 mmol) in a microwave reaction vial was mixed with ethyl formate (6 mL). The vial was capped and heated to 70 °C overnight. After reaction residual ethyl formate was evaporated under reduced pressure. The crude product was purified by silica gel flash column chromatography (methanol in dichloromethane 1−3%) to give the product N-(3-phenylpropyl)formamide. Oil, 98% yield. ^{1}H NMR (500 MHz, $CDCl_3$) δ 8.15−7.96 (m, 1H), 7.33−7.24 (m, 2H), 7.24−7.12 (m, 3H), 6.18−5.73 (m, 1H), 3.35−3.17 (m, 2H), 2.69−2.60 (m, 2H), 1.89−1.78 (m, 2H). ^{13}C NMR (126 MHz, $CDCl_3$) δ 170.33, 164.88, 161.44, 141.51, 141.27, 140.65, 128.67, 128.55, 128.52, 128.42, 128.41, 126.32, 126.13, 126.07, 41.15, 39.39, 37.84, 33.36, 33.22, 32.60, 32.54, 31.17, 31.16, 23.31.

*1. Procedure for the Synthesis of Compound **40**.*

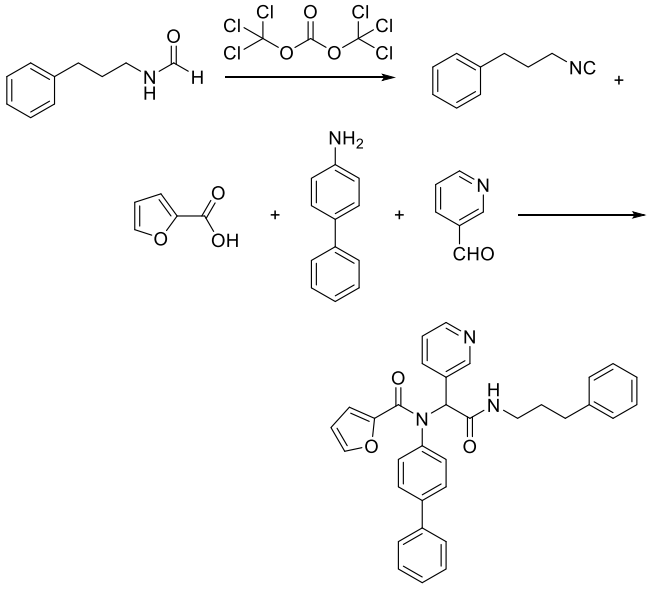

40

To solution of N-(3-phenylpropyl)formamide (2 mmol) in dichloromethane (50 mL) was added triethylamine (4.8 mmol). The solution was cooled to approximately −10 °C using an ethanol ice bath. Triphosgene (0.4 mmol) was added to the stirring mixture. The resulting mixture was stirred at −10 °C for 10 min. In a separate 250 mL round-bottomed flask, 4-aminobiphneyl (2 mmol) and 3-pyridinecarboxaldehyde (2 mmol) were mixed in methanol (100 mL) and stirred at room temperature for 30 min. Then carboxylic acid (2 mmol) and the resulting isocyanide solution (1.0 equiv) were added sequentially, and the resulting mixture was stirred at room temperature overnight. After that, the solvent was removed under reduced pressure and the crude product was purified with flash silica gel chromatography (methanol in dichloromethane 1−5%) to give the final product.

*a. N-tert-Butyl-2-[N-(4-tert-butylphenyl)-1-(furan-2-yl)-formamido]-2-(pyridin-3-yl)acetamide (**1**).* Light yellow solid, 81% yield. ^{1}H NMR (400 MHz, DMSO-d_6) δ 8.38−8.24 (m, 2H), 7.86 (s, 1H), 7.69−7.66 (m, 1H), 7.37 (dt, J = 7.9, 2.0 Hz, 1H), 7.26−7.17 (m, 2H), 7.26−7.02 (br s, 1H), 7.14−7.04 (m, 2H), 6.31 (dd, J = 3.6, 1.7 Hz, 1H), 6.15 (s, 1H), 5.24 (d, J = 3.5 Hz, 1H), 1.22 (s, 9H), 1.19 (s, 9H). ^{13}C NMR (101 MHz, DMSO-d_6) δ 168.1, 158.1, 151.1, 150.9, 148.5, 146.4, 145.2, 137.3, 136.5, 131.2, 130.8, 125.2, 122.7, 115.8, 111.2, 62.3, 50.4, 34.3, 31.0, 28.3. $C_{26}H_{31}N_3O_3$, HRMS calculated for m/z [M + H]$^+$: 434.24437, found 434.2438. HPLC purity: 97%.

*b. 2-[N-(4-tert-Butylphenyl)-1-(furan-2-yl)formamido]-N-(propan-2-yl)-2-(pyridin-3-yl)acetamide (**2**).* White solid. 82% yield. ^{1}H NMR (400 MHz, DMSO-d_6) δ 8.37−8.28 (m, 2H), 8.10 (d, J = 7.5 Hz, 1H), 7.76−7.61 (m, 1H), 7.37 (dt, J = 7.9, 2.0 Hz, 1H), 7.30−7.17 (m, 2H), 7.24−7.00 (br s, 1H), 7.17−7.07 (m, 2H), 6.30 (dd, J = 3.6, 1.7 Hz, 1H), 6.15 (s, 1H), 5.26 (d, J = 3.6 Hz, 1H), 3.99−3.76 (m, 1H), 1.20 (s, 9H), 1.07 (d, J = 6.6 Hz, 3H), 0.95 (d, J = 6.5 Hz, 3H). ^{13}C NMR (101 MHz, DMSO-d_6) δ 167.6, 158.2, 151.1, 151.0, 148.6, 146.3, 145.2, 137.4, 136.5, 131.0, 130.7, 125.2, 122.8, 115.8, 111.2, 62.1, 40.8, 34.3, 31.0, 22.0, 22.0. $C_{25}H_{29}N_3O_3$, HRMS calculated for m/z [M + H]$^+$: 420.2287 (calculated), 420.2282 (found). HPLC purity: 98%.

*c. 2-[N-(4-tert-Butylphenyl)-1-(furan-2-yl)formamido]-N-cyclopropyl-2-(pyridin-3-yl)acetamide (**3**).* White solid. 80% yield. ^{1}H NMR (400 MHz, DMSO-d_6) δ 8.34−8.28 (m, 3H), 7.67 (dd, J = 1.7, 0.7 Hz, 1H), 7.37 (dt, J = 8.0, 1.9 Hz, 1H), 7.26−7.19 (m, 2H), 7.25−6.94 (br s, 1H), 7.16−7.09 (m, 2H), 6.31 (dd, J = 3.6, 1.7 Hz, 1H), 6.09 (s, 1H), 5.28 (dd, J = 3.6, 0.8 Hz, 1H), 2.71−2.60 (m, 1H), 1.20 (s, 9H), 0.67−0.53 (m, 2H), 0.40−0.25 (m, 2H).^{13}C NMR (101 MHz, DMSO-d_6) δ 169.8, 158.2, 151.1, 148.7, 146.3, 145.2, 137.4, 136.4, 130.7, 125.3, 122.8, 115.4, 111.2, 62.0, 34.3, 31.0, 22.0, 5.1. $C_{25}H_{27}N_3O_3$, HRMS calculated for m/z [M + H]$^+$: 418.2131 (calculated), 418.2125 (found). HPLC purity: 96%.

*d. 2-[N-(4-tert-Butylphenyl)-1-(furan-2-yl)formamido]-2-(pyridin-3-yl)-N-(2,4,4-trimethylpentan-2-yl)acetamide (**4**).* Light yellow solid. 60% yield. ^{1}H NMR (500 MHz, DMSO-d_6) δ 8.36−8.28 (m, 2H), 7.79−7.59 (m, 2H), 7.43−7.35 (m, 1H), 7.32-6.97 (br s, 1H), 7.30−7.18 (m, 2H), 7.12 (dd, J = 8.0, 4.8 Hz, 1H), 6.36−6.26 (m, 1H), 6.18 (s, 1H), 5.25 (d, J = 3.6 Hz, 1H), 1.67 (dd, J = 75.5, 14.6 Hz, 2H), 1.35−1.23 (m, 7H), 1.21 (s, 9H), 0.86 (s, 9H). ^{13}C NMR (101 MHz, DMSO-d_6) δ 167.6, 158.0, 151.1, 150.9, 148.5, 146.3, 145.1, 137.4, 136.6, 131.0, 130.8, 125.2, 122.5, 115.7, 111.2, 62.4, 54.3, 50.6, 34.2, 31.1, 31.1, 31.1, 31.0, 28.9, 28.3. $C_{30}H_{39}N_3O_3$, HRMS calculated for m/z [M + H]$^+$: 490.3069 (calculated), 490.3064 (found). HPLC purity: 97%.

*e. 2-[N-(4-tert-Butylphenyl)-1-(furan-2-yl)formamido]-N-cyclopentyl-2-(pyridin-3-yl)acetamide (**5**).* White solid. 85% yield. ^{1}H NMR (400 MHz, DMSO-d_6) δ 8.36−8.28 (m, 2H), 8.18 (d, J = 7.0 Hz, 1H), 7.70−7.65 (m, 1H), 7.37 (dt, J = 7.9, 2.0 Hz, 1H), 7.28−7.18 (m, 2H), 7.25−6.94 (br s, 1H) 7.18−7.06 (m, 2H), 6.30 (dd, J = 3.6, 1.7 Hz, 1H), 6.16 (s, 1H), 5.26 (d, J = 3.6 Hz, 1H), 4.02 (h, J = 6.9 Hz, 1H), 1.86−1.67 (m, 2H), 1.65−1.31 (m, 5H), 1.30−1.21 (m, 1H), 1.20 (s, 9H). ^{13}C NMR (101 MHz, DMSO-d_6) δ 168.1, 158.2, 151.1, 151.0, 148.6, 146.3, 145.2, 137.3, 136.5, 131.0, 130.7, 125.2, 122.8, 115.8, 111.2, 62.0, 50.6, 34.3, 32.0, 31.8, 31.0, 23.5, 23.4. $C_{27}H_{31}N_3O_3$, HRMS calculated for m/z [M + H]$^+$: 446.2443 (calculated), 446.2438 (found). HPLC purity: 100%.

*f. 2-[N-(4-tert-Butylphenyl)-1-(furan-2-yl)formamido]-N-cyclohexyl-2-(pyridin-3-yl)acetamide (**6**).* White solid. 81% yield. ^{1}H NMR (500 MHz, DMSO-d_6) δ 8.36−8.30 (m, 2H), 8.09 (d, J = 7.7 Hz, 1H), 7.67 (dd, J = 1.7, 0.7 Hz, 1H), 7.38 (dt, J = 7.9, 2.0 Hz, 1H), 7.28−7.02 (br s, 1H), 7.25−7.19 (m, 2H), 7.17−7.10 (m, 2H), 6.31 (dd, J = 3.6, 1.7 Hz, 1H), 6.18 (s, 1H), 5.28 (d, J = 3.6 Hz, 1H), 3.63−3.52 (m, 1H), 1.86−1.40 (m, 4H), 1.32−1.14 (m, 13H), 1.14−0.92 (m, 2H). ^{13}C NMR (101 MHz, DMSO-d_6) δ 167.6, 157.9, 151.1, 151.0, 148.6, 146.3, 145.2, 137.3, 136.5, 131.0, 130.7, 125.2, 122.7, 116.2, 111.2, 62.0, 47.9, 34.2, 32.0, 31.0, 25.1, 24.5, 24.3. $C_{28}H_{33}N_3O_3$,

https://doi.org/10.1021/acs.jmedchem.1c00509
J. Med. Chem. 2022, 65, 2848−2865

HRMS calculated for m/z [M + H]$^+$: 460.2600 (calculated), 460.2595 (found). HPLC purity: 96%.

*g. 2-[N-(4-tert-Butylphenyl)-1-(furan-2-yl)formamido]-N-(4-fluorophenyl)-2-(pyridin-3-yl)acetamide (**7**).* Brown solid. 86% yield. ^{1}H NMR (400 MHz, MeOD-d_4) δ 8.43 (d, J = 2.3 Hz, 1H), 8.34 (dd, J = 4.9, 1.6 Hz, 1H), 7.63 (dt, J = 8.0, 2.0 Hz, 1H), 7.59−7.53 (m, 2H), 7.52 (d, J = 1.8 Hz, 1H), 7.45−6.60 (br s, 2H), 7.30 (s, 2H), 7.25−7.17 (m, 1H), 7.08−6.98 (m, 2H), 6.37 (s, 1H), 6.25 (dd, J = 3.6, 1.7 Hz, 1H), 5.46 (d, J = 3.6 Hz, 1H), 1.26 (s, 9H). ^{13}C NMR (101 MHz, MeOD-d_4) δ 169.5, 161.4, 153.8, 152.2, 149.9, 147.4, 146.7, 140.3, 139.4, 137.4, 134.5, 132.2, 131.9, 127.1, 125.5, 123.1, 123.0, 118.4, 116.4, 116.2, 112.3, 65.5, 35.5, 31.6. $C_{28}H_{26}FN_3O_3$, HRMS calculated for m/z [M + H]$^+$: 472.2036 (calculated), 472.2031 (found). HPLC purity: 98%.

*h. 2-[N-(4-tert-Butylphenyl)-1-(furan-2-yl)formamido]-N-(4-methoxyphenyl)-2-(pyridin-3-yl)acetamide (**8**).* Brown solid. 79% yield. ^{1}H NMR (400 MHz, DMSO-d_6) δ 10.22 (s, 1H), 8.42 (d, J = 2.3 Hz, 1H), 8.34 (dd, J = 4.8, 1.6 Hz, 1H), 7.72−7.67 (m, 1H), 7.54−7.46 (m, 2H), 7.43 (dt, J = 8.0, 2.0 Hz, 1H), 7.35−7.05 (br s, 2H), 7.27−7.21 (m, 2H), 7.17−7.10 (m, 1H), 6.92−6.83 (m, 2H), 6.32 (dd, J = 3.6, 1.7 Hz, 1H), 6.30 (s, 1H), 5.29 (d, J = 3.6 Hz, 1H), 3.71 (s, 3H), 1.20 (s, 9H). ^{13}C NMR (101 MHz, DMSO-d_6) δ 167.3, 158.3, 155.3, 151.3, 151.2, 149.0, 146.2, 145.4, 137.5, 136.3, 131.9, 130.8, 130.2, 125.4, 122.9, 120.7, 116.0, 113.9, 111.8, 62.7, 55.1, 34.3, 31.0. $C_{29}H_{29}N_3O_4$, HRMS calculated for m/z [M + H]$^+$: 484.2236 (calculated), 484.2231 (found). HPLC purity: 96%.

*i. 2-[N-(4-tert-Butylphenyl)-1-(furan-2-yl)formamido]-N-(2,6-dimethylphenyl)-2-(pyridin-3-yl)acetamide (**9**).* Light yellow solid. 75% yield. ^{1}H NMR (400 MHz, DMSO-d_6) δ 9.66 (s, 1H), 8.48 (s, 1H), 8.37 (d, J = 4.9 Hz, 1H), 7.70 (dd, J = 1.7, 0.7 Hz, 1H), 7.50 (dt, J = 8.0, 2.0 Hz, 1H), 7.28−7.08 (br s, 2H), 7.28−7.21 (m, 2H), 7.21−7.13 (m, 1H), 7.10−6.99 (m, 3H), 6.35 (s, 1H), 6.32 (dd, J = 3.6, 1.7 Hz, 1H), 5.28 (dd, J = 3.6, 0.8 Hz, 1H), 2.07 (s, 6H), 1.21 (s, 9H). ^{13}C NMR (101 MHz, DMSO-d_6) δ 167.7, 158.3, 151.4, 151.2, 149.0, 146.2, 145.3, 137.7, 136.4, 135.4, 134.6, 130.8, 130.2, 127.6, 126.5, 125.4, 122.7, 115.9, 111.2, 62.6, 34.3, 31.0, 17.9. $C_{30}H_{31}N_3O_3$, HRMS calculated for m/z [M + H]$^+$: 482.2443 (calculated), 482.2438 (found). HPLC purity: 98%.

*j. N-[(1H-1,2,3-Benzotriazol-1-yl)methyl]-2-[N-(4-tert-butylphenyl)-1-(furan-2-yl)formamido]-2-(pyridin-3-yl)acetamide (**10**).* Yellow solid. 22% yield. ^{1}H NMR (500 MHz, $CDCl_3$) δ 8.80 (t, J = 6.7 Hz, 1H), 8.50−8.46 (m, 1H), 8.40−8.36 (m, 1H), 8.10 (d, J = 8.3 Hz, 1H), 8.02 (d, J = 8.6 Hz, 1H), 7.63−7.55 (m, 1H), 7.52−7.38 (m, 3H), 7.24 (s, 1H), 7.12−6.83 (m, 3H), 6.38 (s, 1H), 6.33−6.20 (m, 3H), 5.47−5.40 (m, 2H), 1.37 (s, 9H). ^{13}C NMR (126 MHz, $CDCl_3$) δ 169.8, 159.8, 152.7, 151.6, 149.7, 146.0, 145.9, 145.3, 138.3, 136.1, 132.5, 130.1, 129.6, 127.9, 126.2, 124.4, 122.9, 119.6, 117.5, 111.3, 111.0, 63.0, 51.4, 34.7, 31.3. $C_{29}H_{28}N_6O_3$, HRMS calculated for m/z [M + H]$^+$: 509.2301 (calculated), 509.2296 (found). HPLC purity: 96%.

*k. 2-[N-(4-tert-Butylphenyl)-1-(furan-2-yl)formamido]-N-[(4-methylbenzenesulfonyl)methyl]-2-(pyridin-3-yl)acetamide (**11**).* Yellow solid. 49% yield. ^{1}H NMR (400 MHz, DMSO-d_6) δ 9.28−9.20 (m, 1H), 8.37 (dd, J = 4.3, 2.2 Hz, 1H), 8.23 (s, 1H), 7.69 (dd, J = 1.8, 0.7 Hz, 1H), 7.56−7.49 (m, 2H), 7.30−7.26 (m, 2H), 7.24−7.17 (m, 2H), 7.15−7.05 (m, 2H), 6.96 (s, 2H), 6.31 (dd, J = 3.6, 1.7 Hz, 1H), 6.23 (s, 1H), 5.26 (d, J = 3.6 Hz, 1H), 4.93 (dd, J = 14.1, 7.5 Hz, 1H), 4.61 (dd, J = 14.1, 5.6 Hz, 1H), 2.34 (s, 3H), 1.20 (s, 9H). ^{13}C NMR (101 MHz, DMSO-d_6) δ 169.3, 158.1, 151.4, 151.2, 148.9, 146.1, 145.4, 144.4, 137.7, 136.0, 134.4, 130.7, 129.5, 128.4, 125.3, 122.6, 116.0, 111.8, 61.6, 60.1, 34.3, 30.9, 21.0. $C_{30}H_{31}N_3O_5S$, HRMS calculated for m/z [M + H]$^+$: 546.2062 (calculated), 546.2057 (found). HPLC purity: 96%.

*l. N-Benzyl-2-[N-(4-tert-butylphenyl)-1-(furan-2-yl)formamido]-2-(pyridin-3-yl)acetamide (**12**).* Light yellow solid. 49% yield. ^{1}H NMR (400 MHz, DMSO-d_6) δ 8.74 (t, J = 5.9 Hz, 1H), 8.37−8.31 (m, 2H), 7.72−7.66 (m, 1H), 7.39 (dt, J = 8.0, 1.9 Hz, 1H), 7.33−7.18 (m, 7H), 7.21−7.05 (br s, 1H), 7.17−7.08 (m, 2H), 6.31 (dd, J = 3.6, 1.7 Hz, 1H), 6.22 (s, 1H), 5.28 (d, J = 4.21 Hz, 1H), 4.42−4.27 (m, 2H), 1.21 (s, 9H). ^{13}C NMR (101 MHz, DMSO-d_6) ^{13}C NMR (101 MHz, DMSO) δ 168.9, 158.2, 151.3, 151.1, 148.8, 146.3, 145.3, 139.1, 137.6, 136.5, 130.7, 128.1, 127.1, 126.7, 125.3, 122.7, 115.9, 111.2, 62.4, 42.3, 34.3, 31.0. $C_{29}H_{29}N_3O_3$, HRMS calculated for m/z [M + H]$^+$: 468.2287 (calculated), 468.2282 (found). HPLC purity: 98%.

*m. 2-[N-(4-tert-Butylphenyl)-1-(furan-2-yl)formamido]-N-[(1S)-1-phenylethyl]-2-(pyridin-3-yl)acetamide (**13**).* Light yellow solid. 84% yield. ^{1}H NMR (400 MHz, DMSO−D_6) δ 8.68 (dd, J = 7.8, 2.7 Hz, 1H), 8.41−8.23 (m, 2H), 7.67 (ddd, J = 5.7, 1.7, 0.7 Hz, 1H), 7.46−7.24 (m, 3H), 7.28−6.94 (br s, 1H), 7.23−7.11 (m, 5H), 7.11−7.01 (m, 2H), 6.34−6.24 (m, 2H), 5.28 (dd, J = 3.6, 0.8 Hz, 0.5H), 5.22 (dd, J = 3.6, 0.8 Hz, 0.5H), 5.04−4.91 (m, 1H), 1.37 (d, J = 7.0 Hz, 1.5H), 1.25 (d, J = 7.0 Hz, 1.5H), 1.19 (d, J = 6.0 Hz, 9H). ^{13}C NMR (101 MHz, DMSO) δ 168.1, 167.9, 158.2, 158.1, 151.3, 151.2, 151.0, 148.7, 146.3, 146.2, 145.2, 145.2, 144.3, 144.0, 137.5, 137.4, 136.4, 136.3, 130.8, 130.4, 128.1, 128.0, 126.6, 126.5, 126.1, 125.7, 125.2, 122.8, 122.5, 115.8, 115.8, 111.2, 111.2, 62.0, 48.3, 48.2, 34.2, 31.0, 30.9, 22.2, 22.1. $C_{30}H_{31}N_3O_3$, HRMS calculated for m/z [M + H]$^+$: 482.2443 (calculated), 482.2438 (found). HPLC purity: 97%.

*n. 2-[1-(Furan-2-yl)-N-[4-(trimethylsilyl)phenyl]formamido]-N-[(1S)-1-phenylethyl]-2-(pyridinyl)acetamide (**14**).* Light yellow solid. 50% yield. ^{1}H NMR (500 MHz, $CDCl_3$) δ 8.50−8.41 (m, 2H), 7.47 (dd, J = 49.6, 8.2 Hz, 1H), 7.39−7.16 (m, 8H), 7.10−6.81 (m, 4H), 6.25 (d, J = 13.4 Hz, 1H), 6.18−6.13 (m, 1H), 5.50−5.45 (m, 0.5H), 5.44−5.39 (m, 0.5H), 5.22−5.12 (m, 1H), 1.54 (d, J = 6.9 Hz, 1.5H), 1.48 (d, J = 7.0 Hz, 1.5H), 0.23 (s, 9H). ^{13}C NMR (126 MHz, $CDCl_3$) δ 168.0, 167.7, 159.8, 159.7, 151.5, 151.4, 149.8, 149.7, 146.2, 146.2, 145.1, 145.1, 143.1, 142.1, 142.0, 139.7, 139.5, 138.4, 138.1, 134.1, 134.1, 130.2, 130.1, 130.0, 129.8, 128.7, 128.6, 127.4, 127.3, 126.3, 126.1, 122.9, 122.9, 117.4, 117.4, 111.3, 111.3, 63.4, 62.9, 49.5, 49.5, 22.0, 21.9, 0.1. $C_{29}H_{31}N_3O_3Si$, HRMS calculated for m/z [M + H]$^+$: 498.2212 (calculated), 498.2220 (found). HPLC purity: 96%.

*o. 2-{N-[4-(tert-Butoxy)phenyl]-1-(furan-2-yl)formamido}-N-[(1S)-1-phenylethyl]-2-(pyridin-3-yl)acetamide (**15**).* Yellow solid. 75% yield. ^{1}H NMR (500 MHz, DMSO-d_6) δ 8.72 (t, J = 8.17 Hz, 1H), 8.31 (dd, J = 55, 2.4 Hz, 1H), 8.33 (ddd, J = 13.5, 4.8, 1.6 Hz, 1H), 7.69 (ddd, J = 7.0, 1.7, 0.8 Hz, 1H), 7.50-7.00 (br s, 1H), 7.42-7.06 (m, 3H), 7.43−7.32 (m, 1H), 7.31−7.12 (m, 3H), 6.76 (s, 3H), 6.34 (ddd, J = 8.2, 3.6, 1.7 Hz, 1H), 6.27 (d, J = 13.2 Hz, 1H), 5.46 (d, J = 3.6 Hz, 0.5H), 5.41 (d, J = 3.6 Hz, 0.5H), 5.05−4.94 (m, 1H), 1.38 (d, J = 7.1 Hz, 1.5H), 1.25 (d, J = 7.0 Hz, 1.5H), 1.19 (d, J = 9.5 Hz, 9H). ^{13}C NMR (126 MHz, DMSO-d_6) δ 168.3, 168.1, 166.3, 158.2, 158.1, 154.7, 154.7, 151.4, 151.4, 148.7, 146.4, 146.3, 145.3, 145.3, 144.3, 144.0, 137.6, 137.6, 134.1, 134.1, 132.0, 130.7, 130.3, 128.2, 128.1, 126.7, 126.6, 126.2, 125.7, 123.7, 122.9, 122.6, 116.1, 116.0, 111.2, 111.2, 78.3, 62.0, 48.4, 48.2, 28.4, 22.3, 22.1. $C_{30}H_{31}N_3O_4$, HRMS calculated for m/z [M + H]$^+$: 498.2392 (calculated), 498.2387 (found). HPLC purity: 97%.

*p. 2-[1-(Furan-2-yl)-N-[4-(piperidin-1-yl)phenyl]formamido]-N-[(1S)-1-phenylethyl]-2-(pyridin-3-yl)acetamide (**16**).* Light brown solid. 78% yield. ^{1}H NMR (400 MHz, DMSO-d_6) δ 8.65 (dd, J = 7.8, 3.6 Hz, 1H), 8.40−8.19 (m, 2H), 7.70 (ddd, J = 6.3, 1.7, 0.7 Hz, 1H), 7.64-7.01 (br s, 1H), 7.48−7.29 (m, 3H), 7.28−7.03 (m, 4H), 6.68 (s, 3H), 6.35−6.28 (m, 1H), 6.25 (d, J = 7.8 Hz, 1H), 5.30−5.23 (m, 0.5H), 5.22−5.13 (m, 0.5H), 4.98 (h, J = 7.1 Hz, 1H), 3.11−3.02 (m, 4H), 1.53 (s, 6H), 1.37 (d, J = 7.0 Hz, 1.5H), 1.24 (d, J = 7.0 Hz, 1.5H). ^{13}C NMR (101 MHz, DMSO-d_6) δ 168.3, 168.1, 158.5, 158.5, 151.3, 151.2, 150.8, 148.7, 146.4, 146.3, 145.1, 145.1, 144.3, 144.0, 137.6, 137.6, 131.7, 128.8, 128.7, 128.1, 128.0, 126.6, 126.5, 126.1, 125.7, 115.7, 115.7, 114.5, 111.3, 62.0, 54.9, 48.6, 48.3, 48.1, 30.6, 25.7, 24.9, 24.9, 24.1, 23.7, 22.3. $C_{31}H_{32}N_4O_3$, HRMS calculated for m/z [M + H]$^+$: 509.2552 (calculated), 509.2547 (found). HPLC purity: 97%.

*q. 2-[N-(4-Cyclohexylphenyl)-1-(furan-2-yl)formamido]-N-[(1S)-1-phenylethyl]-2-(pyridin-3-yl)acetamide (**17**).* White solid. 83% yield. ^{1}H NMR (400 MHz, DMSO-d_6) δ 8.68 (dd, J = 7.7, 3.4 Hz, 1H), 8.32 (dd, J = 10.5, 4.7 Hz, 1H), 8.31 (d, J = 48 Hz, 1H), 7.70−7.64 (m, 1H), 7.44−7.28 (m, 3H), 7.28−7.11 (m, 4H), 7.10−6.98 (m, 4H),6.33−6.24 (m, 2H), 5.25 (d, J = 3.6 Hz, 0.5H), 5.20 (d, J =

https://doi.org/10.1021/acs.jmedchem.1c00509
J. Med. Chem. 2022, 65, 2848−2865

3.6 Hz, 0.5H), 5.05−4.91 (m, 1H), 2.48−2.31 (m, 1H), 1.84−1.57 (m, 5H), 1.39-1.10 (m, 5H), 1.31 (dd, J = 41.17, 7.02 Hz, 3H) ^{13}C NMR (101 MHz, DMSO-d_6) δ 168.1, 167.9, 158.2, 158.1, 151.3, 151.2, 148.7, 147.8, 146.3, 146.2, 145.2, 145.2, 144.3, 144.0, 137.5, 136.6, 136.6, 131.1, 128.1, 128.0, 126.7, 126.6, 126.5, 126.1, 125.7, 115.8, 115.8, 111.2, 62.0, 48.3, 48.2, 43.1, 33.8, 33.8, 33.7, 26.1, 25.4, 22.2, 22.1. $C_{32}H_{33}N_3O_3$, HRMS calculated for m/z [M + H]$^+$: 508.2600 (calculated), 508.2595 (found). HPLC purity: 98%.

*r. 2-[1-(Furan-2-yl)-N-[4-(furan-2-yl)phenyl]formamido]-N-[(1S)-1-phenylethyl]-2-(pyridin-3-yl)acetamide (**18**).* Light brown solid. 35% yield. ^{1}H NMR (500 MHz, DMSO-d_6) δ 8.80 (dd, J = 13.9, 7.8 Hz, 1H), 8.66−8.45 (m, 2H), 7.82 (dt, J = 8.1, 1.9 Hz, 1H), 7.71 (dddd, J = 24.9, 6.9, 1.8, 0.8 Hz, 2H), 7.64−7.46 (m, 3H), 7.45−7.07 (m, 7H), 6.96 (ddd, J = 5.9, 3.4, 0.8 Hz, 1H), 6.62−6.55 (m, 1H), 6.38 (d, J = 11.7 Hz, 1H), 6.35 (ddd, J = 8.2, 3.6, 1.7 Hz, 1H), 5.66 (dd, J = 2.8 Hz, 0.8 Hz, 0.5H), 5.62 (d, J = 3.6, 0.8 Hz, 0.5H), 5.06−4.94 (m, 1H), 1.37 (d, J = 7.0 Hz, 1.5H), 1.29 (d, J = 7.0 Hz, 1.5H). ^{13}C NMR (126 MHz, DMSO-d_6) δ 167.4, 167.2, 158.2, 158.2, 151.9, 148.3, 148.2, 146.2, 146.1, 145.5, 145.5, 144.1, 143.8, 143.4, 141.3, 141.1, 138.1, 138.0, 132.4, 132.0, 131.6, 131.6, 130.0, 128.2, 128.1, 126.7, 126.6, 126.1, 125.8, 124.4, 124.1, 123.5, 116.6, 116.6, 112.2, 111.4, 111.4, 107.0, 61.9, 48.5, 48.3, 22.2, 21.9. $C_{30}H_{25}N_3O_4$, HRMS calculated for m/z [M + H]$^+$: 492.1923 (calculated), 492.1918 (found). HPLC purity: 98%.

*s. 2-[1-(Furan-2-yl)-N-[4-(thiophen-2-yl)phenyl]formamido]-N-[(1S)-1-phenylethyl]-2-(pyridin-3-yl)acetamide (**19**).* Light yellow solid. 81% yield. ^{1}H NMR (500 MHz, DMSO-d_6) δ 8.79−8.71 (m, 1H), 8.48−8.23 (m, 2H), 7.74−7.64 (m, 1H), 7.58−7.45 (m, 4H), 7.44−7.31 (m, 3H), 7.30−7.14 (m, 4H), 7.14−7.05 (m, 3H), 6.40−6.28 (m, 2H), 5.63−5.69 (m, 0.5H), 5.58−5.54 (m, 0.5H), 5.07−4.96 (m, 1H), 1.39 (d, J = 7.1 Hz, 1.5H), 1.26 (d, J = 7.0 Hz, 1.5H). ^{13}C NMR (126 MHz, DMSO-d_6) δ 168.1, 167.9, 158.2, 158.1, 151.4, 151.3, 148.9, 146.3, 146.2, 145.4, 145.3, 144.2, 143.9, 142.0, 138.2, 138.2, 137.6, 137.6, 133.4, 133.3, 133.3, 131.9, 130.6, 130.2, 128.6, 128.5, 128.2, 128.1, 126.6, 126.6, 126.2, 126.1, 126.1, 125.7, 125.1, 124.4, 124.4, 123.0, 122.8, 116.3, 116.3, 111.3, 111.3, 62.02, 62.00, 48.3, 48.2, 22.3, 22.1. $C_{30}H_{25}N_3O_3S$, HRMS calculated for m/z [M + H]$^+$: 508.1694 (calculated), 508.1689 (found). HPLC purity: 96%.

*t. 2-[1-(Furan-2-yl)-N-[4-(1H-pyrrol-1-yl)phenyl]formamido]-N-[(1S)-1-phenylethyl]-2-(pyridin-3-yl)acetamide (**20**).* Yellow solid. 80% yield. ^{1}H NMR (400 MHz, DMSO-d_6) δ 8.76 (dd, J = 7.8, 4.0 Hz, 1H), 8.37 (d, J = 51.9 Hz 1H), 8.34 (dd, J = 12.0, 4.4 Hz, 1H), 7.72−7.66 (m, 1H), 7.57−7.30 (m, 7H), 7.30−7.12 (m, 4H), 7.11−7.05 (m, 2 H), 6.38−6.30 (m, 2H), 6.23 (dt, J = 5.2, 2.2 Hz, 2H), 5.58 (d, J = 3.6 Hz, 0.5H), 5.53 (d, J = 3.6 Hz, 0.5H), 5.01 (h, J = 7.3 Hz, 1H), 1.39 (d, J = 7.0 Hz, 1.5H), 1.26 (d, J = 7.0 Hz, 1.5H). ^{13}C NMR (101 MHz, DMSO-d_6) δ 168.3, 168.1, 158.3, 158.2, 151.5, 151.4, 148.9, 146.3, 146.3, 145.5, 145.4, 144.3, 144.0, 139.1, 139.1, 137.7, 137.6, 135.8, 135.7, 132.6, 128.2, 128.1, 126.7, 126.7, 126.2, 125.8, 118.7, 118.3, 116.4, 116.4, 111.4, 110.9, 110.9, 61.9, 54.9, 48.4, 48.3, 22.3, 22.2. $C_{30}H_{26}N_4O_3$, HRMS calculated for m/z [M + H]$^+$: 491.2083 (calculated), 491.2078 (found). HPLC purity: 100%.

*u. 2-[1-(Furan-2-yl)-N-[4-(pyridin-2-yl)phenyl]formamido]-N-[(1S)-1-phenylethyl]-2-(pyridin-3-yl)acetamide (**21**).* Yellow solid. 88% yield. ^{1}H NMR (500 MHz, DMSO-d_6) δ 8.77 (dd, J = 7.8, 5.8 Hz, 1H), 8.65−8.59 (m, 1H), 8.46-8.27 (m, 2H), 7.97−7.88 (m, 3H), 7.88−7.78 (m, 1H), 7.68 (ddd, J = 7.6, 1.7, 0.8 Hz, 1H), 7.57−7.00 (m, 10H), 6.36 (d, J = 14.4 Hz, 1H), 6.32 (ddd, J = 9.0, 3.6, 1.7 Hz, 1H), 5.59 (d, J = 3.6, 0.8 Hz, 0.5H), 5.54 (d, J = 3.6, 0.8 Hz, 0.5H), 5.09−4.94 (m, 1H), 1.39 (d, J = 7.0 Hz, 1.5H), 1.27 (d, J = 7.0 Hz, 1.5H). ^{13}C NMR (126 MHz, DMSO-d_6) δ 168.2, 168.0, 158.2, 158.1, 154.6, 151.4, 151.3, 149.5, 149.5, 149.0, 148.9, 146.3, 146.3, 145.4, 145.4, 144.3, 144.0, 139.9, 139.9, 138.0, 137.7, 137.7, 137.3, 137.3, 131.6, 130.6, 130.3, 128.2, 128.1, 126.7, 126.6, 126.5, 126.2, 125.8, 123.1, 122.9, 122.8, 120.3, 120.3, 116.4, 116.4, 111.43, 111.41, 62.1, 48.4, 48.3, 22.3, 22.1. $C_{31}H_{26}N_4O_3$, HRMS calculated for m/z [M + H]$^+$: 503.2083 (calculated), 503.2078 (found). HPLC purity: 98%.

*v. 2-[N-(4-Benzylphenyl)-1-(furan-2-yl)formamido]-N-[(1S)-1-phenylethyl]-2-(pyridin-3-yl)acetamide (**22**).* White solid. 80% yield. ^{1}H NMR (400 MHz, DMSO-d_6) δ 8.71 (dd, J = 7.8, 4.2 Hz, 1H), 8.44−8.23 (m, 2H), 7.66 (ddd, J = 5.5, 1.7, 0.7 Hz, 1H), 7.45−7.31 (m, 3H), 7.31−7.11 (m, 7H), 7.10−6.96 (m, 6H), 6.39−6.18 (m, 2H), 5.43−5.38 (m, 0.5H), 5.36−5.30 (m, 0.5H), 5.06−4.89 (m, 1H), 3.86 (d, J = 6.6 Hz, 2H), 1.37 (d, J = 7.0 Hz, 1.5H), 1.25 (d, J = 7.0 Hz, 1.5H). ^{13}C NMR (101 MHz, DMSO-d_6) δ 168.1, 167.9, 158.2, 158.1, 151.4, 151.3, 148.8, 146.3, 146.3, 145.2, 145.2, 144.2, 143.9, 141.1, 140.9, 137.5, 137.1, 137.0, 131.3, 130.7, 130.3, 129.2, 128.4, 128.4, 128.3, 128.3, 128.2, 128.0, 126.6, 126.6, 126.1, 125.9, 125.9, 125.7, 122.9, 122.6, 116.0, 116.0, 111.1, 62.0, 48.3, 48.2, 40.2, 22.3, 22.1. $C_{33}H_{29}N_3O_3$, HRMS calculated for m/z [M + H]$^+$: 516.2287 (calculated), 516.2282 (found). HPLC purity: 98%.

*w. 2-(N-{[1,1′-Biphenyl]-4-yl}-1-(furan-2-yl)formamido)-N-[(1S)-1-phenylethyl]-2-(pyridin-3-yl)acetamide (**23**).* White solid. 89% yield. ^{1}H NMR (400 MHz, DMSO-d_6) δ 8.75 (dd, J = 7.8, 5.0 Hz, 1H), 8.53−8.21 (m, 2H), 7.72−7.66 (m, 1H), 7.66−7.58 (m, 2H), 7.58−7.24 (m, 10H), 7.24−7.05 (m, 4H), 6.47−6.23 (m, 2H), 5.63−5.53 (m, 0.5H), 5.52−5.43 (m, 0.5H), 5.10−4.92 (m, 1H), 1.39 (d, J = 7.0 Hz, 1.5H), 1.27 (d, J = 7.0 Hz, 1.5H). ^{13}C NMR (101 MHz, DMSO-d_6) δ 168.1, 167.9, 158.2, 158.1, 151.3, 151.3, 148.9, 146.3, 146.2, 145.3, 145.3, 144.2, 143.9, 139.4, 138.55, 138.50, 138.4, 137.6, 131.8, 128.95, 128.93, 128.2, 128.0, 127.8, 126.6, 126.6, 126.5, 126.4, 126.1, 125.7, 116.2, 116.2, 111.3, 62.1, 48.4, 48.3, 22.2, 22.1. $C_{32}H_{27}N_3O_3$, HRMS calculated for m/z [M + H]$^+$: 502.2130 (calculated), 502.2132 (found). HPLC purity: 97%.

*x. (2R)-2-(N-{[1,1′-Biphenyl]-4-yl}-1-(furan-2-yl)formamido)-N-[(1S)-1-phenylethyl]-2-(pyridin- 3-yl)acetamide (**23R, Jun8-76-3A**).* White solid, 45% yield. ^{1}H NMR (500 MHz, DMSO-d6) δ 8.74 (d, J = 7.9 Hz, 1H), 8.43 (d, J = 2.3 Hz, 1H), 8.35 (dd, J = 4.8, 1.6 Hz, 1H), 7.71−7.66 (m, 1H), 7.66−7.61 (m, 2H), 7.60−7.52 (m, 2H), 7.50 (dt, J = 8.0, 2.0 Hz, 1H), 7.46−7.32 (m, 8H), 7.30−7.15 (m, 3H), 6.36 (s, 1H), 6.32 (dd, J = 3.6, 1.7 Hz, 1H), 5.50 (d, J = 3.6 Hz, 1H), 5.02 (p, J = 7.1 Hz, 1H), 1.27 (d, J = 7.0 Hz, 3H). ^{13}C NMR (126 MHz, DMSO-d6) δ 168.1, 158.1, 151.3, 148.9, 146.2, 145.3, 143.9, 139.4, 138.5, 138.5, 137.6, 131.8, 130.7, 128.9, 128.2, 127.8, 126.6, 126.5, 126.4, 126.1, 123.0, 116.2, 111.3, 62.1, 48.2, 22.1. $C_{32}H_{27}N_3O_3$, HRMS calculated for m/z [M + H]$^+$: 502.2130 (calculated), 502.2132 (found). HPLC purity: 100%.

*y. (2S)-2-(N-{[1,1′-**b**iphenyl]-4-yl}-1-(furan-2-yl)formamido)-N-[(1S)-1-phenylethyl]-2-(pyridin-3- yl)acetamide (**23S**).* White solid, 45% yield. ^{1}H NMR (500 MHz, DMSO-d6) δ 8.75 (d, J = 7.6 Hz, 1H), 8.38−8.25 (m, 2H), 7.73−7.66 (m, 1H), 7.66−7.59 (m, 2H), 7.53 (d, J = 8.0 Hz, 2H), 7.47−7.31 (m, 4H), 7.30−7.13 (m, 5H), 7.12−7.06 (m, 3H), 6.36−6.32 (m, 2H), 5.54 (d, J = 3.6 Hz, 1H), 5.00 (p, J = 7.1 Hz, 1H), 1.38 (d, J = 7.0 Hz, 3H). ^{13}C NMR (126 MHz, DMSO) δ 168.0, 158.2, 151.4, 148.9, 146.3, 145.4, 144.3, 139.4, 138.5, 138.5, 137.6, 131.8, 130.3, 128.9, 128.1, 127.8, 126.6, 126.5, 126.5, 125.8, 122.7, 116.3, 111.4, 62.1, 48.4, 22.3. $C_{32}H_{27}N_3O_3$, HRMS calculated for m/z [M + H]$^+$: 502.2130 (calculated), 502.2132 (found). HPLC purity: 97%.

*z. 2-(N-{[1,1′-Biphenyl]-4-yl}-1-(1H-imidazol-4-yl)formamido)-N-[(1S)-1-phenylethyl]-2-(pyridin-3-yl)acetamide (**24**).* White solid. 38% yield. ^{1}H NMR (500 MHz, DMSO-d_6) δ 12.76 (s, 1H), 8.74 (d, J = 7.9 Hz, 1H), 8.44 (d, J = 2.4 Hz, 1H), 8.36 (dd, J = 4.8, 1.7 Hz, 1H), 7.73−7.32 (br s, 1H), 7.68−7.60 (m, 3H), 7.60−7.49 (m, 3H), 7.48−7.23 (m, 9H), 7.19 (ddd, J = 7.8, 4.8, 0.8 Hz, 1H), 6.40 (s, 1H), 5.53 (s, 1H), 5.03 (p, J = 7.2 Hz, 1H), 1.26 (d, J = 7.0 Hz, 3H). ^{13}C NMR (126 MHz, DMSO-d_6) δ 168.3, 151.3, 148.8, 144.0, 139.6, 138.6, 137.6, 137.0, 132.1, 130.9, 128.9, 128.2, 127.8, 126.6, 126.5, 126.1, 123.0, 62.0, 48.2, 22.2. $C_{31}H_{27}N_5O_2$, HRMS calculated for m/z [M + H]$^+$: 502.2242 (calculated), 502.2238 (found). HPLC purity: 96%.

*aa. 2-(N-{[1,1′-Biphenyl]-4-yl}-1-(1,2-oxazol-5-yl)formamido)-N-[(1S)-1-phenylethyl]-2-(pyridin-3-yl)acetamide (**25**).* Light yellow solid. 82% yield. ^{1}H NMR (400 MHz, DMSO-d_6) δ 8.83 (dd, J = 7.7, 5.7 Hz, 1H), 8.56−8.26 (m, 3H), 7.65−7.45 (m, 5H), 7.44−7.06 (m, 11H), 6.35 (d, J = 11.2 Hz, 1H), 5.88−5.77 (m, 1H), 5.13−4.94 (m, 1H), 1.40 (d, J = 7.0 Hz, 1.5H), 1.28 (d, J = 7.0 Hz, 1.5H). ^{13}C NMR (101 MHz, DMSO-d_6) δ 167.5, 167.3, 161.7, 161.6, 157.0, 157.0, 151.4, 151.3, 150.7, 149.1, 144.1, 143.8, 139.7, 138.4, 137.6, 137.4, 137.3, 131.4, 130.1, 129.7, 128.9, 128.9, 128.2, 128.1, 127.9,

https://doi.org/10.1021/acs.jmedchem.1c00509
J. Med. Chem. 2022, 65, 2848−2865

126.7, 126.7, 126.56, 126.54, 126.1, 125.8, 123.1, 122.8, 107.11, 107.10, 62.3, 48.5, 48.4, 22.3, 22.1. $C_{31}H_{26}N_4O_3$, HRMS calculated for m/z $[M + H]^+$: 503.2083 (calculated), 503.2078 (found). HPLC purity: 98%.

*ab. 2-(N-{[1,1′-Biphenyl]-4-yl}-1-(1,3-oxazol-5-yl)formamido)-N-[(1S)-1-phenylethyl]-2-(pyridin-3-yl)acetamide (**26**).* Yellow solid. 85% yield. ^{1}H NMR (400 MHz, DMSO-d_6) δ 8.80 (dd, J = 7.8, 4.7 Hz, 1H), 8.57−8.23 (m, 3H), 7.69−7.49 (m, 5H), 7.48−7.32 (m, 6H), 7.31−7.07 (m, 5H), 6.34 (d, J = 9.3 Hz, 1H), 5.87 (d, J = 16.3 Hz, 1H), 5.02 (h, J = 7.6 Hz, 1H), 1.40 (d, J = 7.0 Hz, 1.5H), 1.27 (d, J = 7.0 Hz, 1.5H). ^{13}C NMR (101 MHz, DMSO-d_6) δ 167.8, 167.6, 156.9, 156.8, 153.69, 153.65, 151.4, 151.3, 149.1, 144.2, 144.24, 144.21, 143.9, 140.1, 138.4, 137.6, 137.6, 137.5, 137.4, 131.8, 130.4, 130.3, 129.9, 128.9, 128.9, 128.2, 128.1, 127.9, 126.8, 126.7, 126.65, 126.64, 126.1, 125.7, 123.1, 122.8, 62.1, 48.4, 48.3, 22.2, 22.1. $C_{31}H_{26}N_4O_3$, HRMS calculated for m/z $[M + H]^+$: 503.2083 (calculated), 503.2078 (found). HPLC purity: 97%.

*ac. N-tert-Butyl-2-[N-(4-tert-butylphenyl)-1-(furan-2-yl)-formamido]-2-(pyrazin-2-yl)acetamide (**27**).* Light yellow solid. 86% yield. ^{1}H NMR (500 MHz, DMSO-d_6) δ 8.53 (dd, J = 2.5, 1.5 Hz, 1H), 8.47 (d, J = 1.5 Hz, 1H), 8.43 (d, J = 2.6 Hz, 1H), 8.00 (s, 1H), 7.68 (dd, J = 1.7, 0.7 Hz, 1H), 7.35−7.16 (m, 4H), 6.33 (dd, J = 3.6, 1.7 Hz, 1H), 6.28 (s, 1H), 5.39 (d, J = 3.6 Hz, 1H), 1.22 (s, 9H), 1.14 (s, 9H). ^{13}C NMR (126 MHz, DMSO-d_6) δ 166.0, 158.3, 152.0, 151.0, 146.2, 145.3, 145.2, 143.6, 143.0, 136.9, 130.2, 125.2, 116.0, 111.2, 65.1, 50.5, 34.3, 31.0, 28.1. $C_{25}H_{30}N_4O_3$, HRMS calculated for m/z $[M + H]^+$: 435.2396 (calculated), 435.2391 (found). HPLC purity: 96%.

*ad. N-tert-Butyl-2-[N-(4-tert-butylphenyl)-1-(furan-2-yl)-formamido]-2-(1H-imidazol-4-yl)acetamide (**28**).* Light yellow solid. 60% yield. ^{1}H NMR (400 MHz, DMSO-d_6) δ 8.91 (d, J = 1.3 Hz, 1H), 8.02 (s, 1H), 7.73−7.66 (m, 1H), 7.36−7.29 (m, 2H), 7.23 (dd, J = 1.3, 0.7 Hz, 3H), 6.34 (dd, J = 3.6, 1.7 Hz, 1H), 6.27 (s, 1H), 5.34 (d, J = 3.6 Hz, 1H), 1.24 (s, 9H), 1.23 (s, 9H). ^{13}C NMR (101 MHz, DMSO-d_6) δ 165.4, 158.2, 151.4, 146.0, 145.5, 136.4, 134.5, 129.9, 128.3, 125.5, 119.6, 116.2, 111.4, 56.2, 50.7, 34.4, 31.0, 28.2. $C_{24}H_{30}N_4O_3$, HRMS calculated for m/z $[M + H]^+$: 423.2396 (calculated), 423.2391 (found). HPLC purity: 97%.

*ae. N-tert-Butyl-2-[N-(4-tert-butylphenyl)-1-(furan-2-yl)-formamido]-2-(pyrimidin-5-yl)acetamide (**29**).* Yellow solid. 78% yield. ^{1}H NMR (400 MHz, DMSO-d_6) δ 8.93 (s, 1H), 8.46 (s, 2H), 7.95 (s, 1H), 7.68 (dd, J = 1.7, 0.8 Hz, 1H), 7.33-7.12 (br s, 2H)7.27 (d, J = 8.0 Hz, 2H), 6.32 (dd, J = 3.6, 1.7 Hz, 1H), 6.16 (s, 1H), 5.32 (d, J = 3.6 Hz, 1H), 1.22 (s, 9H), 1.21 (s, 9H). ^{13}C NMR (101 MHz, DMSO-d_6) δ 167.1, 158.1, 157.8, 157.2, 151.3, 146.2, 145.3, 136.4, 130.7, 129.6, 125.5, 116.0, 111.3, 60.5, 50.5, 34.3, 30.9, 28.2. $C_{25}H_{30}N_4O_3$, HRMS calculated for m/z $[M + H]^+$: 435.2396 (calculated), 435.2391 (found). HPLC purity: 98%.

*af. 2-(N-{[1,1′-Biphenyl]-4-yl}-1-(furan-2-yl)formamido)-N-cyclopropyl-2-(pyridin-3-yl)acetamide (**30**).* Light yellow solid. 89% yield. ^{1}H NMR (500 MHz, DMSO-d_6) δ 8.46−8.26 (m, 3H), 7.69 (dd, J = 1.7, 0.8 Hz, 1H), 7.66−7.62 (m, 2H), 7.62−7.50 (m, 2H), 7.49-7.14 (br s, 1H), 7.48−7.31 (m, 5H), 7.17 (dd, J = 7.9, 4.8 Hz, 1H), 6.34 (dd, J = 3.6, 1.7 Hz, 1H), 6.18 (s, 1H), 5.55 (dd, J = 3.6, 0.8 Hz, 1H), 2.74−2.65 (m, 1H), 0.73−0.55 (m, 2H), 0.46−0.26 (m, 2H). ^{13}C NMR (126 MHz, DMSO-d_6) δ 169.9, 158.2, 151.1, 148.9, 146.3, 145.4, 139.5, 138.5, 138.5, 137.5, 131.7, 130.6, 128.9, 127.8, 126.5, 126.5, 123.0, 116.3, 111.3, 62.0, 22.5, 5.6, 5.5. $C_{27}H_{23}N_3O_3$, HRMS calculated for m/z $[M + H]^+$: 438.1817 (calculated), 438.1812 (found). HPLC purity: 98%.

*ag. 2-(N-{[1,1′-Biphenyl]-4-yl}-1-(furan-2-yl)formamido)-2-(pyridin-3-yl)-N-(2,4,4-trimethylpentan-2-yl)acetamide (**31**).* Light yellow solid. 62% yield. ^{1}H NMR (400 MHz, DMSO-d_6) δ 8.48−8.22 (m, 2H), 7.75−7.66 (m, 2H), 7.66−7.60 (m, 2H), 7.60−7.49 (m, 2H), 7.51-7.09 (br s, 1H), 7.49−7.30 (m, 5H), 7.15 (ddd, J = 7.9, 4.8, 0.8 Hz, 1H), 6.32 (dd, J = 3.6, 1.7 Hz, 1H), 6.25 (s, 1H), 5.49 (dd, J = 3.6, 0.8 Hz, 1H), 1.68 (dd, J = 75.4, 14.5 Hz, 2H), 1.29 (d, J = 16.4 Hz, 6H), 0.87 (s, 9H). ^{13}C NMR (101 MHz, DMSO-d_6) δ 167.7, 158.0, 151.3, 148.6, 146.3, 145.2, 139.4, 138.6, 138.6, 137.6, 131.9, 130.9, 128.9, 127.8, 126.5, 126.4, 122.8, 116.1, 111.3, 62.4, 50.7, 31.2, 31.1, 29.0, 28.4. $C_{32}H_{35}N_3O_3$, HRMS calculated for m/z $[M + H]^+$: 510.2756 (calculated), 510.2751 (found). HPLC purity: 100%.

*ah. 2-(N-{[1,1′-Biphenyl]-4-yl}-1-(furan-2-yl)formamido)-N-cyclopentyl-2-(pyridin-3-yl)acetamide (**32**).* White solid. 78% yield. ^{1}H NMR (400 MHz, DMSO-d_6) δ 8.35 (d, J = 20.6 Hz, 2H), 8.24 (d, J = 7.0 Hz, 1H), 7.68 (dd, J = 1.7, 0.7 Hz, 1H), 7.66−7.60 (m, 2H), 7.55 (d, J = 8.1 Hz, 2H), 7.51-7.12 (br s, 1H), 7.50−7.29 (m, 5H), 7.16 (dd, J = 7.9, 4.7 Hz, 1H), 6.33 (dd, J = 3.6, 1.7 Hz, 1H), 6.24 (s, 1H), 5.53 (d, J = 3.6 Hz, 1H), 4.06 (h, J = 6.6 Hz, 1H), 1.90−1.70 (m, 2H), 1.68−1.37 (m, 5H), 1.33−1.19 (m, 1H). ^{13}C NMR (101 MHz, DMSO-d_6) δ 168.2, 158.2, 151.2, 148.8, 146.3, 145.3, 139.4, 138.5, 137.5, 131.7, 130.9, 128.9, 127.8, 126.5, 126.4, 123.0, 116.2, 111.3, 62.0, 50.7, 32.1, 31.8, 23.5, 23.4. $C_{29}H_{27}N_3O_3$, HRMS calculated for m/z $[M + H]^+$: 466.2130 (calculated), 466.2125 (found). HPLC purity: 96%.

*ai. 2-(N-{[1,1′-Biphenyl]-4-yl}-1-(1H-imidazol-4-yl)formamido)-N-cyclopentyl-2-(pyridin-3-yl)acetamide (**33**).* White solid. 44% yield. ^{1}H NMR (500 MHz, DMSO-d_6) δ 8.38 (d, J = 2.3 Hz, 1H), 8.33 (dd, J = 4.8, 1.7 Hz, 1H), 8.24 (d, J = 7.1 Hz, 1H), 7.82-7.32 (br s, 1H), 7.73−7.55 (m, 5H), 7.53−7.29 (m, 5H), 7.23−7.12 (m, 1H), 6.24 (s, 1H), 5.54 (s, 1H), 4.12−4.00 (m, 1H) 1.90−1.70 (m, 2H), 1.67−1.40 (m, 5H), 1.32−1.19 (m, 1H). ^{13}C NMR (126 MHz, DMSO-d_6) δ 168.4, 151.2, 148.8, 139.6, 138.7, 138.6, 137.5, 132.1, 131.1, 129.0, 127.9, 126.6, 123.0, 62.0, 50.7, 32.1, 31.9, 23.5, 23.4. $C_{28}H_{27}N_5O_2$, HRMS calculated for m/z $[M + H]^+$: 466.2242 (calculated), 466.2238 (found). HPLC purity: 98%.

*aj. 2-(N-{[1,1′-Biphenyl]-4-yl}-1-(furan-2-yl)formamido)-N-cyclohexyl-2-(pyridin-3-yl)acetamide (**34**).* White solid. 83% yield. ^{1}H NMR (500 MHz, $CDCl_3$/ MeOD-d_4) δ 8.43 (s, 1H), 8.38−8.31 (m, 1H), 7.55−7.48 (m, 3H), 7.48−7.27 (m, 6H), 7.26−6.95 (br s, 1H), 7.16−7.05 (m, 2H), 6.22 (s, 1H), 6.16−6.08 (m, 1H), 5.55 (d, J = 3.6 Hz, 1H), 3.79 (s, 1H), 3.77−3.69 (m, 1H), 2.04−1.46 (m, 5H), 1.43−0.9 (m, 5H). ^{13}C NMR (126 MHz, $CDCl_3$/ MeOD-d_4) δ 168.1, 168.0, 159.8, 150.9, 148.9, 145.9, 145.1, 141.5, 139.3, 138.5, 137.9, 131.3, 130.8, 128.8, 127.8, 127.4, 126.8, 123.3, 117.5, 111.3, 62.7, 62.6, 32.5, 32.4, 25.3, 24.8, 24.7. $C_{30}H_{29}N_3O_3$, HRMS calculated for m/z $[M + H]^+$: 480.2287 (calculated), 480.2282 (found). HPLC purity: 97%.

*ak. 2-(N-{[1,1′-Biphenyl]-4-yl}-1-(1H-imidazol-4-yl)formamido)-N-cyclohexyl-2-(pyridin-3-yl)acetamide (**35**).* White solid. 42% yield. ^{1}H NMR (500 MHz, DMSO-d_6) δ 8.40 (d, J = 2.3 Hz, 1H), 8.33 (dd, J = 4.8, 1.7 Hz, 1H), 8.17 (d, J = 7.7 Hz, 1H), 7.89 (s, 1H), 7.69−7.63 (m, 2H), 7.59 (d, J = 7.2 Hz, 2H), 7.54-6.99 (br s, 1 H), 7.51−7.32 (m, 5H), 7.17 (ddd, J = 7.9, 4.8, 0.8 Hz, 1H), 6.26 (s, 1H), 5.56 (s, 1H), 3.67-3.57 (m, 1H), 1.86−1.48 (m, 5H), 1.35−1.16 (m, 3H), 1.15−0.96 (m, 2H). ^{13}C NMR (126 MHz, DMSO-d_6) δ 167.8, 159.8, 151.2, 148.8, 139.8, 138.5, 138.4, 137.6, 136.8, 132.0, 130.9, 129.0, 127.9, 126.7, 126.6, 123.0, 62.1, 48.0, 32.1, 25.1, 24.5, 24.4. $C_{29}H_{29}N_5O_2$, HRMS calculated for m/z $[M + H]^+$: 480.2399 (calculated), 480.2394 (found). HPLC purity: 96%.

*al. 2-[N-(4-Cyclohexylphenyl)-1-(1,2-oxazol-5-yl)formamido]-N-[(1S)-1-phenylethyl]-2-(pyridin-3-yl)acetamide (**36**).* Yellow solid. 76% yield. ^{1}H NMR (400 MHz, DMSO-d_6) δ 8.69 (dd, J = 7.8, 3.1 Hz, 1H), 8.32 (ddd, J = 10.3, 4.8, 1.6 Hz, 1H), 8.31 (dd, J = 46.3, 2.2 Hz, 1H), 7.74−7.60 (m, 1H), 7.46−7.29 (m, 3H), 7.28−6.96 (m, 7H), 6.35−6.19 (m, 2H), 5.26−5.22 (m, 0.5H), 5.21−5.15 (m, 0.5H), 5.08−4.87 (m, 1H), 2.48−2.34 (m, 1H), 1.87−1.59 (m, 5H), 1.47−1.07 (m, 5H), 1.31 (dd, J = 47.0 7.0 Hz, 3 H) ^{13}C NMR (101 MHz, DMSO-d_6) δ 168.2, 167.9, 158.2, 158.1, 151.3, 151.3, 148.8, 147.8, 146.3, 146.2, 145.3, 145.2, 144.3, 144.0, 137.5, 136.6, 136.6, 131.1, 130.7, 130.4, 128.2, 128.0, 126.7, 126.6, 126.6, 126.1, 125.7, 122.8, 122.5, 115.8, 115.8, 111.2, 62.0, 54.9, 48.3, 48.2, 43.1, 33.8, 33.8, 33.7, 26.1, 25.4, 22.3, 22.1. $C_{31}H_{32}N_4O_3$, HRMS calculated for m/z $[M + H]^+$: 509.2552 (calculated), 509.2547 (found). HPLC purity: 97%.

*am. 2-(N-{[1,1′-Biphenyl]-4-yl}-1-(1H-imidazol-4-yl)formamido)-N-[(1S)-1-phenylethyl]-2-(pyrazin-2-yl)acetamide (**37**).* Yellow solid. 42% yield. ^{1}H NMR (500 MHz, DMSO-d_6) δ 8.89−8.37 (m, 5H), 7.70−7.61 (m, 3H), 7.57 (dd, J = 16.7, 8.1 Hz, 2H), 7.52−7.41 (m, 3H), 7.40−7.29 (m, 4H), 7.29−7.16 (m, 3H), 6.61−6.47 (m, 1H),

https://doi.org/10.1021/acs.jmedchem.1c00509
J. Med. Chem. 2022, 65, 2848−2865

5.07−4.93 (m, 1H), 1.33 (d, J = 7.0 Hz, 1.5H), 1.30 (d, J = 7.0 Hz, 1.5H). ^{13}C NMR (126 MHz, DMSO-d_6) δ 166.7, 166.5, 151.4, 151.3, 146.1, 146.0, 144.2, 144.1, 143.8, 143.7, 143.4, 138.7, 131.6, 131.5, 129.0, 128.2, 128.1, 127.9, 126.6, 126.6, 126.1, 126.0, 64.5, 48.4, 48.3, 22.2, 22.2. $C_{30}H_{26}N_6O_2$, HRMS calculated for m/z [M + H]$^+$: 503.2195 (calculated), 503.2190 (found). HPLC purity: 99%.

*an. 2-(N-{[1,1′-Biphenyl]-4-yl}-1-(furan-2-yl)formamido)-N-[(1S)-1-phenylethyl]-2-(pyrazin-2-yl)acetamide (**38**).* Yellow solid. 83% yield. ^{1}H NMR (500 MHz, DMSO-d_6) δ 8.79 (dd, J = 24.5, 7.8 Hz, 1H), 8.68−8.34 (m, 3H), 7.72−7.67 (m, 1H), 7.66−7.61 (m, 2H), 7.60−7.51 (m, 2H), 7.49-7.26 (br s, 1H), 7.48−7.41 (m, 2H), 7.39−7.30 (m, 4H), 7.29−7.16 (m, 3H), 6.56−6.46 (m, 1H), 6.40−6.31 (m, 1H), 5.66−5.64 (m, 0.5H), 5.62−5.59 (m, 0.5H), 5.10−4.90 (m, 1H), 1.39−1.24 (m, 3H). ^{13}C NMR (126 MHz, DMSO-d_6) δ 166.5, 166.3, 158.3, 158.3, 151.2, 151.1, 146.2, 146.1, 146.0, 145.5, 145.4, 144.1, 144.0, 143.8, 143.7, 143.4, 139.6, 139.5, 138.8, 138.8, 138.6, 138.6, 131.2, 131.1, 129.0, 128.2, 128.1, 127.9, 126.7, 126.6, 126.1, 126.0, 116.6, 116.5, 111.4, 111.4, 64.5, 64.4, 48.5, 48.4, 22.2. $C_{31}H_{26}N_4O_3$, HRMS calculated for m/z [M + H]$^+$: 503.2083 (calculated), 503.2078 (found). HPLC purity: 100%.

*ao. 2-(N-{[1,1′-Biphenyl]-4-yl}-1-(furan-2-yl)formamido)-N-(2,2-diphenylethyl)-2-(pyrazin-2-yl)acetamide (**39**).* Yellow solid. 65% yield. ^{1}H NMR (500 MHz, DMSO-d_6) δ 8.39−8.19 (m, 3H), 7.69 (dd, J = 1.7, 0.7 Hz, 1H), 7.67−7.60 (m, 2H), 7.58−7.50 (m, 2H), 7.46−7.42 (m, 2H), 7.38−7.33 (m, 1H), 7.32−7.10 (m, 12H), 7.05 (dt, J = 7.9, 2.0 Hz, 1H), 6.96 (dd, J = 8.0, 4.8 Hz, 1H), 6.33 (dd, J = 3.6, 1.7 Hz, 1H), 6.21 (s, 1H), 5.52 (dd, J = 3.6, 0.8 Hz, 1H), 4.23 (t, J = 7.9 Hz, 1H), 4.06−3.90 (m, 1H), 3.73−3.57 (m, 1H). ^{13}C NMR (126 MHz, DMSO-d_6) δ 168.7, 158.2, 151.4, 148.5, 146.3, 145.3, 142.7, 142.6, 139.4, 138.5, 138.5, 137.4, 131.6, 130.5, 129.0, 128.4, 128.3, 127.9, 127.8, 127.8, 126.5, 126.5, 126.3, 126.3, 122.7, 116.3, 111.3, 62.1, 50.0, 43.6. $C_{38}H_{31}N_3O_3$, HRMS calculated for m/z [M + H]$^+$: 578.2443 (calculated), 578.2438 (found). HPLC purity: 96%.

*ap. 2-(N-{[1,1′-Biphenyl]-4-yl}-1-(furan-2-yl)formamido)-N-(3-phenylpropyl)-2-(pyridin-3-yl)acetamide (**40**).* Light yellow solid. 76% yield. ^{1}H NMR (500 MHz, DMSO-d_6) δ 8.55 (d, J = 2.2 Hz, 1H), 8.49 (dd, J = 5.2, 1.6 Hz, 1H), 8.32 (t, J = 5.5 Hz, 1H), 7.89−7.79 (m, 1H), 7.64 (d, J = 1.5 Hz, 1H), 7.63−7.51 (m, 4H), 7.49−7.42 (m, 1H), 7.42−7.21 (m, 5H), 7.21−7.13 (m, 2H), 7.12−7.06 (m, 3H), 6.30 (dd, J = 3.6, 1.7 Hz, 1H), 6.19 (s, 1H), 5.58 (d, J = 3.5 Hz, 1H), 3.08 (q, J = 6.6 Hz, 2H), 2.48−2.39 (m, 2H), 1.69−1.55 (m, 2H). ^{13}C NMR (101 MHz, DMSO-d_6) δ 167.7, 158.3, 146.1, 145.5, 141.6, 139.7, 138.8, 138.5, 132.8, 131.2, 128.9, 128.2, 128.2, 127.9, 126.8, 126.6, 125.7, 124.5, 116.6, 111.4, 62.6, 38.6, 32.4, 30.7. $C_{33}H_{29}N_3O_3$, HRMS calculated for m/z [M + H]$^+$: 516.2287 (calculated), 516.2282 (found). HPLC purity: 98%.

Native Mass Spectrometry. Prior to analysis, the protein was buffer exchanged into 0.2 M ammonium acetate (pH 6.8) and diluted to 10 μM. DTT was dissolved in water and prepared at a 400 mM stock. Each ligand was dissolved in ethanol and diluted to 10× stock concentrations. The final mixture was prepared by adding 4 μL of protein, 0.5 μL of DTT stock, and 0.5 μL of ligand stock for a final concentration of 4 mM DTT and 70 μM protein. The final ligand concentrations were 10 μM and 30 μM. The mixtures were then incubated for 10 min at room temperature prior to analysis. Each sample was mixed and analyzed in triplicate.

Native mass spectrometry (MS) was performed using a Q-Exactive HF quadrupole-Orbitrap mass spectrometer with the Ultra-High Mass Range research modifications (Thermo Fisher Scientific). Samples were ionized using nanoelectrospray ionization in positive ion mode using 1.0 kV capillary voltage at a 150 °C capillary temperature. The samples were all analyzed with a 1,000−25,000 m/z range, the resolution set to 30,000, and a trapping gas pressure set to 3. Between 10 and 50 V of source fragmentation was applied to all samples to aid in desolvation. Data were deconvolved and analyzed with UniDec.[28]

Enzymatic Assays. The main protease (M^{pro}) enzymatic assays were carried out in M^{pro} reaction buffer containing 20 mM HEPES pH 6.5, 120 mM NaCl, 0.4 mM EDTA, 20% glycerol, and 4 mM DTT, and the SARS-CoV-2 papain-like protease (PL^{pro}) enzymatic assays were carried out in PL^{Pro} reaction buffer containing 50 mM HEPES, pH7.5, 0.01% triton-100, and 5 mM DTT. The percentage of inhibition and enzymatic IC_{50} values were calculated as previously described.[7,8] Briefly, the assay was performed in 96-well plates with 100 μL of 100 nM M^{pro} protein or 200 nM PL^{Pro} protein in their respective reaction buffers. Then 1 μL testing compound at various concentrations was added to each well and incubated at 30 °C for 30 min. The enzymatic reaction was initiated by adding 1 μL of 1 mM corresponding FRET substrate (the final substrate concentration is 10 μM). The reaction was monitored in a Cytation 5 image reader with filters for excitation at 360/40 nm and emission at 460/40 nm at 30 °C for 1 h. The initial velocity of the enzymatic reaction with and without testing compounds was calculated by linear regression for the first 15 min of the kinetic progress curve.

For the Morrison plot, 10 μL of 100 nM SARS-CoV-2 M^{pro} protein was added to 190 μL of M^{pro} reaction buffer containing testing compound and the FRET substrate, and the reaction was monitored for 2 h. The final FRET substrate concentration in this assay is 20 μM. Detailed curve fitting and K_I determination were described previously.[7,8]

For Michaelis−Menten and Lineweaver−Burk plots, assay was carried out as follows: 50 μL of 50 μM M^{pro} protein was added to 50 μL of reaction buffer containing testing compound and various concentrations of FRET substrate to initiate the enzyme reaction. The initial velocity of the enzymatic reaction with and without testing compounds was calculated by linear regression for the first 15 min of the kinetic progress curve, plotted against substrate concentrations in Prism 8 with the Michaelis−Menten equation.

Cathepsin K and cathepsin L enzymatic assay was carried out as follows: cathepsin K or cathepsin L was activated by incubating in reaction buffer [20 mM sodium acetate, 1 mM EDTA, and 5 mM DTT (pH 5.5)] for 30 min at 30 °C. Upon activation, the assay was assembled in 96-well plates with 100 μL of cathepsin K at 200 pM or cathepsin L at 300 pM in reaction buffer. Then, 1 μL of testing compound at various concentrations was added to each well and incubated at 30 °C for 30 min. The enzymatic reaction was initiated by adding 1 μL of FRET substrate Z-Phe-Arg-AMC (BACHEM, catalog #. 4003379.0050) (the final substrate concentration is about 5 μM for cathepsin K and 1 μM for cathepsin L). The reaction was monitored in a Cytation 5 image reader with filters for excitation at 360/40 nm and emission at 460/40 nm at 30 °C for 1 h. The IC_{50} values were calculated as described in the previous section.

Calpain 1 enzymatic assay was carried out as follows: 1 μL of 1 μg/μL calpain 1 protein was added to 100 μL of calpain I reaction buffer [50 mM HEPES, 50 mM NaCl, and 10 mM DTT and 5 mM $CaCl_2$ (pH 7.5)]; the enzymatic reaction was iniated by adding 1 μL of 4 mM N-succinyl-Leu-Leu-Val-Tyr-7-amido-4-methylcoumarin substrate (Sigma-Aldrich catalog #. S6510). The reaction was monitored with a Cytation 5 image reader with filters for excitation at 360/40 nm and emission at 460/40 nm at 30 °C for 1 h. The IC_{50} values were calculated as described in the previous section.

Trypsin enzymatic assay was carried out in a 50 μL volume containing 100 nM trypsin in 50 mM HEPES (pH7.6) reaction buffer, 100 μM Bz-Arg-AMC·HCl (BACHEM, catalog no. 4002540.0050), and serial concentrations of test compounds in duplicate. The reaction was monitored with a Cytation 5 image reader with filters for excitation at 360/40 nm and emission at 460/40 nm at 30 °C for 1 h. The IC_{50} values were calculated as described in the previous section.

Differential Scanning Fluorimetry (DSF). The thermal shift binding assay (TSA) was carried out using a Thermal Fisher QuantStudio 5 Real-Time PCR System as described previously.[7,8,29] Briefly, 3 μM SARS-CoV-2 M^{pro} protein in M^{pro} reaction buffer was incubated with various concentrations of compound **ML188** or **23R** at 30 °C for 30 min. 1X SYPRO orange dye was added, and the fluorescence of the well was monitored under a temperature gradient range from 20 to 90 °C with a 0.05 °C/s incremental step. Measured T_m was plotted against compound concentration with one-site binding function in Prism 8.

Cytotoxicity Measurement. Evaluation of the cytotoxicity of compounds was carried out using the neutral red uptake assay.[30,31] Briefly, 80,000 cells/mL of the tested cell lines was dispensed into 96-

https://doi.org/10.1021/acs.jmedchem.1c00509
J. Med. Chem. 2022, 65, 2848−2865

well cell culture plates at 100 μL/well. Twenty-four hours later, the growth medium was removed and washed with 150 μL PBS buffer. 200 μL of fresh serum-free medium containing serial diluted compounds was added to each well. After incubating for 5 days at 37 °C, the medium was removed and replaced with 100 μL DMEM medium containing 40 μg/mL neutral red and incubated for 2−4 h at 37 °C. The amount of neutral red taken up was determined by measuring the absorbance at 540 nm using a Multiskan FC Microplate Photometer (Fisher Scientific). The CC_{50} values were calculated from best-fit dose response curves with variable slope in Prism 8.

Immunofluorescence Assay. Antiviral immunofluorescence assay was carried out as previously described.[8] Briefly, Vero E6 cells in 96-well plates (Corning) were infected with SARS-CoV-2 (USA-WA1/2020 isolate) at MOI of 0.05 in DMEM supplemented with 1% FBS. Immediately before the viral inoculation, the tested compounds in a 3-fold dilution concentration series were also added to the wells in triplicate. The infection proceeded for 48 h without the removal of the viruses or the compounds. The cells were then fixed with 4% paraformaldehyde, permeabilized with 0.1% Triton-100, blocked with DMEM containing 10% FBS, and stained with a rabbit monoclonal antibody against SARS-CoV-2 NP (GeneTex, GTX635679) and an Alexa Fluor 488-conjugated goat antimouse secondary antibody (ThermoFisher Scientific). Hoechst 33342 was added in the final step to counterstain the nuclei. Fluorescence images of approximately ten thousand cells were acquired per well with a 10× objective in a Cytation 5 (BioTek). The total number of cells, as indicated by the nuclei staining, and the fraction of the infected cells, as indicated by the NP staining, was quantified with the cellular analysis module of the Gen5 software (BioTek).

Antiviral Assay in Calu-3 Cells. Calu-3 cells (ATCC, HTB-55) grown in Minimal Eagles Medium supplemented with 1% nonessential amino acids, 1% penicillin/streptomycin, and 10% FBS are plated in 384 well plates. The next day, 50 nL of drug suspended in DMSO is added as an 8-pt dose response with 3-fold dilutions between test concentrations in triplicate, starting at 40 μM final concentration. The negative control (DMSO, n = 32) and positive control (10 μM Remdesivir, n = 32) are included on each assay plate. Calu3 cells are pretreated with controls and test drugs (in triplicate) for 2 h prior to infection. In BSL3 containment, SARS-CoV-2 (isolate USA-WA1/2020) diluted in serum free growth medium is added to plates to achieve an MOI = 0.5. Cells are incubated continuously with drugs and SARS-CoV-2 for 48 h. Cells are fixed and then immunstained with anti-dsRNA (J2), and nuclei are counterstained with Hoechst 33342 for automated microscopy. Automated image analysis quantifies the number of cells per well (toxicity) and the percentage of infected cells (dsRNA+ cells/cell number) per well. SARS-CoV-2 infection at each drug concentration was normalized to aggregated DMSO plate control wells and expressed as percentage-of-control (POC = % Infection $_{sample}$/Avg % Infection $_{DMSO\ cont}$). A nonlinear regression curve fit analysis (GraphPad Prism 8) of POC infection and cell viability versus the $\log_{10}$ transformed concentration values to calculate EC_{50} values for infection and CC_{50} values for cell viability. Selectivity index (SI) was calculated as a ratio of drug's CC_{50} and EC_{50} values (SI = CC_{50}/IC_{50}).

M^{pro} Crystallization and Structure Determination. **23R** was added to 20 mg/mL SARS-CoV-2 M^{pro} to a final concentration of 1.75 mM and incubated overnight at 4°C. This mixture was then diluted 4-fold with protein stock buffer (20 mM Tris pH 7.5, 200 mM NaCl, 1 mM DTT) and then spun down at 13,000*g* for 1 min to remove precipitate. Crystals were grown by mixing the protein-inhibitor sample with an equal volume of crystallization buffer (20% PEG 3350, 0.2 M NaF) in a vapor diffusion, hanging drop apparatus. Crystals were then transferred to a drop with crystallization buffer containing 5 mM **23R** for 1 h, followed by a brief soaking in a cryoprotectant solution of 30% PEG 3350 and 15% glycerol with 2 mM **23R**. Crystals were then flash frozen in liquid nitrogen for X-ray diffraction.

X-ray diffraction data for the SARS-CoV-2 M^{pro} structures were collected on the SBC 19-ID beamline at the Advanced Photon Source (APS) in Argonne, IL, and processed with the HKL3000 software suite. The CCP4 versions of MOLREP[32] was used for molecular replacement using a previously solved SARS-CoV-2 M^{pro} structure, 6YB7. Structural refinement was performed using REFMAC5[33] and COOT.[34] The crystallographic statistics is shown in Supporting Information Table S2. The complex structure for SARS-CoV-2 M^{pro} with **23R** has been deposited in the Protein Data Bank with the accession ID of 7KX5 (SARS-CoV-2 M^{Pro} + Jun8-76-3A).

■ ASSOCIATED CONTENT

Supporting Information

The Supporting Information is available free of charge at https://pubs.acs.org/doi/10.1021/acs.jmedchem.1c00509.

Target selectivity of noncovalent inhibitor **23R**; crystallographic statistics; H NMR and C NMR spectra for final products; HPLC traces for representative compounds (PDF)

Molecular formula strings (CSV)

■ AUTHOR INFORMATION

Corresponding Authors

Yu Chen − *Department of Molecular Medicine, Morsani College of Medicine, University of South Florida, Tampa, Florida 33612, United States*; Phone: 813-974-7809; Email: ychen1@usf.edu

Jun Wang − *Department of Pharmacology and Toxicology, College of Pharmacy, The University of Arizona, Tucson, Arizona 85721, United States*; orcid.org/0000-0002-4845-4621; Phone: 520-626-1366; Email: junwang@pharmacy.arizona.edu; Fax: 520-626-0749

Authors

Naoya Kitamura − *Department of Pharmacology and Toxicology, College of Pharmacy, The University of Arizona, Tucson, Arizona 85721, United States*

Michael Dominic Sacco − *Department of Molecular Medicine, Morsani College of Medicine, University of South Florida, Tampa, Florida 33612, United States*

Chunlong Ma − *Department of Pharmacology and Toxicology, College of Pharmacy, The University of Arizona, Tucson, Arizona 85721, United States*

Yanmei Hu − *Department of Pharmacology and Toxicology, College of Pharmacy, The University of Arizona, Tucson, Arizona 85721, United States*

Julia Alma Townsend − *Department of Chemistry and Biochemistry, The University of Arizona, Tucson, Arizona 85721, United States*

Xiangzhi Meng − *Department of Microbiology, Immunology and Molecular Genetics, University of Texas Health Science Center at San Antonio, San Antonio, Texas 78229, United States*

Fushun Zhang − *Department of Microbiology, Immunology and Molecular Genetics, University of Texas Health Science Center at San Antonio, San Antonio, Texas 78229, United States*

Xiujun Zhang − *Department of Molecular Medicine, Morsani College of Medicine, University of South Florida, Tampa, Florida 33612, United States*

Mandy Ba − *Department of Pharmacology and Toxicology, College of Pharmacy, The University of Arizona, Tucson, Arizona 85721, United States*

Tommy Szeto − *Department of Pharmacology and Toxicology, College of Pharmacy, The University of Arizona, Tucson, Arizona 85721, United States*
Adis Kukuljac − *Department of Molecular Medicine, Morsani College of Medicine, University of South Florida, Tampa, Florida 33612, United States*
Michael Thomas Marty − *Department of Chemistry and Biochemistry, The University of Arizona, Tucson, Arizona 85721, United States*
David Schultz − *Department of Biochemistry and Biophysics, University of Pennsylvania, Philadelphia, Pennsylvania 19104, United States*
Sara Cherry − *Department of Pathology and Laboratory Medicine, University of Pennsylvania, Philadelphia, Pennsylvania 19104, United States*
Yan Xiang − *Department of Microbiology, Immunology and Molecular Genetics, University of Texas Health Science Center at San Antonio, San Antonio, Texas 78229, United States*

Complete contact information is available at: https://pubs.acs.org/10.1021/acs.jmedchem.1c00509

Author Contributions

J.W. conceived and designed the study; N.K. synthesized and characterized the compounds; M.S. carried out M^{pro} crystallization and structure determination with the assistance of X.Z. and analyzed the data with Y.C.; C.M. expressed the M^{pro} and PL^{pro} and performed the IC_{50} determination, thermal shift-binding assay, and enzymatic kinetic studies; Y.H. performed the cytotoxicity assay; X.M. and F.Z. performed the SARS-CoV-2 immunofluorescence assay in Vero E6 cells under the guidance of Y.X. D.S. performed the SARS-CoV-2 immunofluorescence assay in Calu-3 cells under the guidance of S.C. J.T. performed the native mass spectrometry experiments with the guidance from M.T.M.; J.W. and Y.C. secured funding and supervised the study; J.W., Y.C., and M.S. wrote the manuscript with input from the others.

Notes

The authors declare the following competing financial interest(s): Naoya Kitamura, Chunlong Ma, Yanmei Hu, and Jun Wang are inventors of a filed patent claiming the use of 23R and related compounds as potential COVID-19 antiviral drugs.

■ ACKNOWLEDGMENTS

This research was partially supported by the National Institutes of Health (NIH) (Grants AI147325 and AI157046) and the Arizona Biomedical Research Centre Young Investigator grant (ADHS18-198859) to J.W. The antiviral assay in Calu-3 cells was conducted through the NIAID preclinical service under a nonclinical evaluation agreement. J.A.T. and M.T.M. were funded by the National Institute of General Medical Sciences and National Institutes of Health (Grant R35 GM128624 to M.T.M.). We thank Michael Kemp for assistance with crystallization and X-ray diffraction data collection. We also thank the staff members of the Advanced Photon Source of Argonne National Laboratory, particularly those at the Structural Biology Center (SBC), with X-ray diffraction data collection. SBC-CAT is operated by UChicago Argonne, LLC, for the U.S. Department of Energy, Office of Biological and Environmental Research under contract DE-AC02-06CH11357. The SARS-CoV-2 experiments were supported by a COVID-19 pilot grant from UTHSCSA and NIH grant AI151638 to Y.X. SARS-Related Coronavirus 2, Isolate USA-WA1/2020 (NR-52281) was deposited by the Centers for Disease Control and Prevention and obtained through BEI Resources, NIAID, NIH.

■ ABBREVIATIONS USED

SARS-CoV-2, severe acute respiratory syndrome coronavirus 2; JAK, janus kinase; Ugi-4CR, Ugi four-component reaction; M^{pro}, main protease; $3CL^{pro}$, 3-chymotrypsin-like protease; Nsp5, nonstructural protein 5; $2A^{pro}$, 2A protease; $3C^{pro}$, 3C protease; PL^{pro}, papain-like protease

■ REFERENCES

(1) Kalil, A. C.; Patterson, T. F.; Mehta, A. K.; Tomashek, K. M.; Wolfe, C. R.; Ghazaryan, V.; Marconi, V. C.; Ruiz-Palacios, G. M.; Hsieh, L.; Kline, S.; Tapson, V.; Iovine, N. M.; Jain, M. K.; Sweeney, D. A.; El Sahly, H. M.; Branche, A. R.; Regalado Pineda, J.; Lye, D. C.; Sandkovsky, U.; Luetkemeyer, A. F.; Cohen, S. H.; Finberg, R. W.; Jackson, P. E. H.; Taiwo, B.; Paules, C. I.; Arguinchona, H.; Goepfert, P.; Ahuja, N.; Frank, M.; Oh, M. D.; Kim, E. S.; Tan, S. Y.; Mularski, R. A.; Nielsen, H.; Ponce, P. O.; Taylor, B. S.; Larson, L.; Rouphael, N. G.; Saklawi, Y.; Cantos, V. D.; Ko, E. R.; Engemann, J. J.; Amin, A. N.; Watanabe, M.; Billings, J.; Elie, M. C.; Davey, R. T.; Burgess, T. H.; Ferreira, J.; Green, M.; Makowski, M.; Cardoso, A.; de Bono, S.; Bonnett, T.; Proschan, M.; Deye, G. A.; Dempsey, W.; Nayak, S. U.; Dodd, L. E.; Beigel, J. H.; Members, A.-S. G.. Baricitinib plus remdesivir for hospitalized adults with Covid-19. *N. Engl. J. Med.* **2021**, *384*, 795−807.
(2) Gil, C.; Ginex, T.; Maestro, I.; Nozal, V.; Barrado-Gil, L.; Cuesta-Geijo, M. A.; Urquiza, J.; Ramirez, D.; Alonso, C.; Campillo, N. E.; Martinez, A. COVID-19: drug targets and potential treatments. *J. Med. Chem.* **2020**, *63*, 12359−12386.
(3) Ullrich, S.; Nitsche, C. The SARS-CoV-2 main protease as drug target. *Bioorg. Med. Chem. Lett.* **2020**, *30*, 127377.
(4) Rut, W.; Groborz, K.; Zhang, L.; Sun, X.; Zmudzinski, M.; Pawlik, B.; Wang, X.; Jochmans, D.; Neyts, J.; Młynarski, W.; Hilgenfeld, R.; Drag, M. SARS-CoV-2 Mpro inhibitors and activity-based probes for patient-sample imaging. *Nat. Chem. Biol.* **2021**, *17*, 222−228.
(5) Ghosh, A. K.; Brindisi, M.; Shahabi, D.; Chapman, M. E.; Mesecar, A. D. Drug development and medicinal chemistry efforts toward SARS-coronavirus and Covid-19 therapeutics. *ChemMedChem* **2020**, *15*, 907−932.
(6) Boras, B.; Jones, R. M.; Anson, B. J.; Arenson, D.; Aschenbrenner, L.; Bakowski, M. A.; Beutler, N.; Binder, J.; Chen, E.; Eng, H.; Hammond, J.; Hoffman, R.; Kadar, E. P.; Kania, R.; Kimoto, E.; Kirkpatrick, M. G.; Lanyon, L.; Lendy, E. K.; Lillis, J. R.; Luthra, S. A.; Ma, C.; Noell, S.; Obach, R. S.; O'Brien, M. N.; O'Connor, R.; Ogilvie, K.; Owen, D.; Pettersson, M.; Reese, M. R.; Rogers, T.; Rossulek, M. I.; Sathish, J. G.; Steppan, C.; Ticehurst, M.; Updyke, L. W.; Zhu, Y.; Wang, J.; Chatterjee, A. K.; Mesecar, A. D.; Anderson, A. S.; Allerton, C. Discovery of a novel inhibitor of coronavirus 3CL protease as a clinical candidate for the potential treatment of COVID-19. *bioRxiv* **2020**, 2020.09.12.293498.
(7) Ma, C.; Sacco, M. D.; Hurst, B.; Townsend, J. A.; Hu, Y.; Szeto, T.; Zhang, X.; Tarbet, B.; Marty, M. T.; Chen, Y.; Wang, J. Boceprevir, GC-376, and calpain inhibitors II, XII inhibit SARS-CoV-2 viral replication by targeting the viral main protease. *Cell Res.* **2020**, *30*, 678−692.
(8) Sacco, M. D.; Ma, C.; Lagarias, P.; Gao, A.; Townsend, J. A.; Meng, X.; Dube, P.; Zhang, X.; Hu, Y.; Kitamura, N.; Hurst, B.; Tarbet, B.; Marty, M. T.; Kolocouris, A.; Xiang, Y.; Chen, Y.; Wang, J. Structure and inhibition of the SARS-CoV-2 main protease reveal strategy for developing dual inhibitors against M(pro) and cathepsin L. *Sci. Adv.* **2020**, *6*, eabe0751.

(9) Rathnayake, A. D.; Zheng, J.; Kim, Y.; Perera, K. D.; Mackin, S.; Meyerholz, D. K.; Kashipathy, M. M.; Battaile, K. P.; Lovell, S.; Perlman, S.; Groutas, W. C.; Chang, K. O. 3C-like protease inhibitors block coronavirus replication in vitro and improve survival in MERS-CoV-infected mice. *Sci. Transl. Med.* **2020**, *12*, eabc5332.
(10) Qiao, J.; Li, Y. S.; Zeng, R.; Liu, F. L.; Luo, R. H.; Huang, C.; Wang, Y. F.; Zhang, J.; Quan, B.; Shen, C.; Mao, X.; Liu, X.; Sun, W.; Yang, W.; Ni, X.; Wang, K.; Xu, L.; Duan, Z. L.; Zou, Q. C.; Zhang, H. L.; Qu, W.; Long, Y. H.; Li, M. H.; Yang, R. C.; Liu, X.; You, J.; Zhou, Y.; Yao, R.; Li, W. P.; Liu, J. M.; Chen, P.; Liu, Y.; Lin, G. F.; Yang, X.; Zou, J.; Li, L.; Hu, Y.; Lu, G. W.; Li, W. M.; Wei, Y. Q.; Zheng, Y. T.; Lei, J.; Yang, S. SARS-CoV-2 M(pro) inhibitors with antiviral activity in a transgenic mouse model. *Science* **2021**, *371*, 1374−1378.
(11) Pedersen, N. C.; Kim, Y.; Liu, H.; Galasiti Kankanamalage, A. C.; Eckstrand, C.; Groutas, W. C.; Bannasch, M.; Meadows, J. M.; Chang, K. O. Efficacy of a 3C-like protease inhibitor in treating various forms of acquired feline infectious peritonitis. *J. Feline Med. Surg.* **2018**, *20*, 378−392.
(12) Kim, Y.; Liu, H.; Galasiti Kankanamalage, A. C.; Weerasekara, S.; Hua, D. H.; Groutas, W. C.; Chang, K. O.; Pedersen, N. C. Reversal of the progression of fatal coronavirus infection in cats by a broad-spectrum coronavirus protease inhibitor. *PLoS Pathog.* **2016**, *12*, e1005531.
(13) Jacobs, J.; Grum-Tokars, V.; Zhou, Y.; Turlington, M.; Saldanha, S. A.; Chase, P.; Eggler, A.; Dawson, E. S.; Baez-Santos, Y. M.; Tomar, S.; Mielech, A. M.; Baker, S. C.; Lindsley, C. W.; Hodder, P.; Mesecar, A.; Stauffer, S. R. Discovery, synthesis, and structure-based optimization of a series of N-(tert-butyl)-2-(N-arylamido)-2-(pyridin-3-yl) acetamides (ML188) as potent non-covalent small molecule inhibitors of the severe acute respiratory syndrome coronavirus (SARS-CoV) 3CL protease. *J. Med. Chem.* **2013**, *56*, 534−46.
(14) Turlington, M.; Chun, A.; Tomar, S.; Eggler, A.; Grum-Tokars, V.; Jacobs, J.; Daniels, J. S.; Dawson, E.; Saldanha, A.; Chase, P.; Baez-Santos, Y. M.; Lindsley, C. W.; Hodder, P.; Mesecar, A. D.; Stauffer, S. R. Discovery of N-(benzo[1,2,3]triazol-1-yl)-N-(benzyl)acetamido)-phenyl) carboxamides as severe acute respiratory syndrome coronavirus (SARS-CoV) 3CLpro inhibitors: Identification of ML300 and noncovalent nanomolar inhibitors with an induced-fit binding. *Bioorg. Med. Chem. Lett.* **2013**, *23*, 6172−6177.
(15) Zaidman, D.; Gehrtz, P.; Filep, M.; Fearon, D.; Prilusky, J.; Duberstein, S.; Cohen, G.; Owen, D.; Resnick, E.; Strain-Damerell, C.; Lukacik, P.; Barr, H.; Walsh, M. A.; von Delft, F.; London, N. An automatic pipeline for the design of irreversible derivatives identifies a potent SARS-CoV-2 Mpro inhibitor. *bioRxiv* **2020**, 2020.09.21.299776.
(16) Zhang, L. L.; Lin, D. Z.; Sun, X. Y. Y.; Curth, U.; Drosten, C.; Sauerhering, L.; Becker, S.; Rox, K.; Hilgenfeld, R. Crystal structure of SARS-CoV-2 main protease provides a basis for design of improved alpha-ketoamide inhibitors. *Science* **2020**, *368*, 409−412.
(17) Zhang, J.; Hu, Y.; Foley, C.; Wang, Y.; Musharrafieh, R.; Xu, S.; Zhang, Y.; Ma, C.; Hulme, C.; Wang, J. Exploring ugi-azide four-component reaction products for broad-spectrum influenza antivirals with a high genetic barrier to drug resistance. *Sci. Rep.* **2018**, *8*, 4653.
(18) Siklos, M.; BenAissa, M.; Thatcher, G. R. J. Cysteine proteases as therapeutic targets: does selectivity matter? A systematic review of calpain and cathepsin inhibitors. *Acta Pharm. Sin. B* **2015**, *5*, 506−519.
(19) Cianni, L.; Feldmann, C. W.; Gilberg, E.; Gutschow, M.; Juliano, L.; Leitao, A.; Bajorath, J.; Montanari, C. A. Can cysteine protease cross-class inhibitors achieve selectivity? *J. Med. Chem.* **2019**, *62*, 10497−10525.
(20) Steuten, K.; Kim, H.; Widen, J. C.; Babin, B. M.; Onguka, O.; Lovell, S.; Bolgi, O.; Cerikan, B.; Cortese, M.; Muir, R. K.; Bennett, J. M.; Geiss-Friedlander, R.; Peters, C.; Bartenschlager, R.; Bogyo, M. Challenges for targeting SARS-CoV-2 proteases as a therapeutic strategy for COVID-19. *ACS Infect. Dis.* **2021**, DOI: 10.1021/acsinfecdis.0c00815.
(21) Ma, Y.; Li, L.; He, S.; Shang, C.; Sun, Y.; Liu, N.; Meek, T. D.; Wang, Y.; Shang, L. Application of dually activated michael acceptor to the rational design of reversible covalent inhibitor for enterovirus 71 3C protease. *J. Med. Chem.* **2019**, *62*, 6146−6162.
(22) Jin, Z.; Du, X.; Xu, Y.; Deng, Y.; Liu, M.; Zhao, Y.; Zhang, B.; Li, X.; Zhang, L.; Peng, C.; Duan, Y.; Yu, J.; Wang, L.; Yang, K.; Liu, F.; Jiang, R.; Yang, X.; You, T.; Liu, X.; Yang, X.; Bai, F.; Liu, H.; Liu, X.; Guddat, L. W.; Xu, W.; Xiao, G.; Qin, C.; Shi, Z.; Jiang, H.; Rao, Z.; Yang, H. Structure of M(pro) from SARS-CoV-2 and discovery of its inhibitors. *Nature* **2020**, *582*, 289−293.
(23) Li, J.; Zhou, X.; Zhang, Y.; Zhong, F.; Lin, C.; McCormick, P. J.; Jiang, F.; Luo, J.; Zhou, H.; Wang, Q.; Fu, Y.; Duan, J.; Zhang, J. Crystal structure of SARS-CoV-2 main protease in complex with the natural product inhibitor shikonin illuminates a unique binding mode. *Sci. Bull. (Beijing)* **2021**, *66*, 661−663.
(24) Ma, C.; Hu, Y.; Townsend, J. A.; Lagarias, P. I.; Marty, M. T.; Kolocouris, A.; Wang, J. Ebselen, disulfiram, carmofur, PX-12, tideglusib, and shikonin are nonspecific promiscuous SARS-CoV-2 main protease inhibitors. *ACS Pharmacol. Transl. Sci.* **2020**, *3*, 1265−1277.
(25) Gurard-Levin, Z. A.; Liu, C.; Jekle, A.; Jaisinghani, R.; Ren, S.; Vandyck, K.; Jochmans, D.; Leyssen, P.; Neyts, J.; Blatt, L. M.; Beigelman, L.; Symons, J. A.; Raboisson, P.; Scholle, M. D.; Deval, J. Evaluation of SARS-CoV-2 3C-like protease inhibitors using self-assembled monolayer desorption ionization mass spectrometry. *Antiviral Res.* **2020**, *182*, 104924.
(26) Musharrafieh, R.; Ma, C.; Zhang, J.; Hu, Y.; Diesing, J. M.; Marty, M. T.; Wang, J. Validating enterovirus D68-2A(pro) as an antiviral drug target and the discovery of telaprevir as a potent D68−2A(pro) inhibitor. *J. Virol.* **2019**, *93*, e02221−18.
(27) Cady, S. D.; Wang, J.; Wu, Y.; DeGrado, W. F.; Hong, M. Specific binding of adamantane drugs and direction of their polar amines in the pore of the influenza M2 transmembrane domain in lipid bilayers and dodecylphosphocholine micelles determined by NMR spectroscopy. *J. Am. Chem. Soc.* **2011**, *133*, 4274−4284.
(28) Marty, M. T.; Baldwin, A. J.; Marklund, E. G.; Hochberg, G. K.; Benesch, J. L.; Robinson, C. V. Bayesian deconvolution of mass and ion mobility spectra: from binary interactions to polydisperse ensembles. *Anal. Chem.* **2015**, *87*, 4370−4376.
(29) Hu, Y.; Meng, X.; Zhang, F.; Xiang, Y.; Wang, J. The in vitro antiviral activity of lactoferrin against common human coronaviruses and SARS-CoV-2 is mediated by targeting the heparan sulfate co-receptor. *Emerging Microbes Infect.* **2021**, *10*, 317−330.
(30) Repetto, G.; del Peso, A.; Zurita, J. L. Neutral red uptake assay for the estimation of cell viability/cytotoxicity. *Nat. Protoc.* **2008**, *3*, 1125−1131.
(31) Ma, C.; Zhang, J.; Wang, J. Pharmacological characterization of the spectrum of antiviral activity and genetic barrier to drug resistance of M2-S31N channel blockers. *Mol. Pharmacol.* **2016**, *90*, 188−98.
(32) Vagin, A.; Teplyakov, A. MOLREP: an automated program for molecular replacement. *J. Appl. Crystallogr.* **1997**, *30*, 1022−1025.
(33) Murshudov, G. N.; Skubak, P.; Lebedev, A. A.; Pannu, N. S.; Steiner, R. A.; Nicholls, R. A.; Winn, M. D.; Long, F.; Vagin, A. A. REFMAC5 for the refinement of macromolecular crystal structures. *Acta Crystallogr., Sect. D: Biol. Crystallogr.* **2011**, *67*, 355−367.
(34) Emsley, P.; Cowtan, K. Coot: model-building tools for molecular graphics. *Acta Crystallogr., Sect. D: Biol. Crystallogr.* **2004**, *60*, 2126−2132.

NOTE ADDED AFTER ASAP PUBLICATION

This paper was published ASAP on April 23, 2021, with errors in Figure 6. These were corrected in the version published ASAP on May 12, 2021.

https://doi.org/10.1021/acs.jmedchem.1c00509
J. Med. Chem. 2022, 65, 2848−2865